Journal of Nonlinear Science (2024) 34:88
https://doi.org/10.1007/s00332-024-10054-2

Journal of Nonlinear Science

Turing Bifurcation in the Swift–Hohenberg Equation on Deterministic and Random Graphs

Georgi S. Medvedev[1] · **Dmitry E. Pelinovsky**[2]

Received: 15 December 2023 / Accepted: 3 June 2024 / Published online: 16 July 2024

Abstract

The Swift–Hohenberg equation (SHE) is a partial differential equation that explains how patterns emerge from a spatially homogeneous state. It has been widely used in the theory of pattern formation. Following a recent study by Bramburger and Holzer (SIAM J Math Anal 55(3):2150–2185, 2023), we consider discrete SHE on deterministic and random graphs. The two families of the discrete models share the same continuum limit in the form of a nonlocal SHE on a circle. The analysis of the continuous system, parallel to the analysis of the classical SHE, shows bifurcations of spatially periodic solutions at critical values of the control parameters. However, the proximity of the discrete models to the continuum limit does not guarantee that the same bifurcations take place in the discrete setting in general, because some of the symmetries of the continuous model do not survive discretization. We use the center manifold reduction and normal forms to obtain precise information about the number and stability of solutions bifurcating from the homogeneous state in the discrete models on deterministic and sparse random graphs. Moreover, we present detailed numerical results for the discrete SHE on the nearest-neighbor and small-world graphs.

Keywords Swift-Hohenberg equation · Turing bifurcation · Cayley graphs · Random graphs · Normal form

Mathematics Subject Classification 35B32 · 35B36 · 37H20 · 37L10 · 82C21

Communicated by Arnd Scheel.

✉ Georgi S. Medvedev
medvedev@drexel.edu

Dmitry E. Pelinovsky
dmpeli@math.mcmaster.ca

[1] Department of Mathematics, Drexel University, 3141 Chestnut Street, Philadelphia, PA 19104, USA

[2] Department of Mathematics and Statistics, McMaster University, Hamilton, ON L8S 4K1, Canada

1 Introduction

Networks of interacting dynamical systems (a.k.a. interacting particle systems) form an important class of models of natural and technological systems. Examples include neuronal networks, swarm of fireflies, coupled lasers, and power grids, to name a few (Dorfler and Bullo 2012; Pikovsky et al. 2001; Porter and Gleeson 2016; Strogatz 2003).

When the number of particles is large, taking a limit as the number of particles goes to infinity is an effective tool for analyzing network dynamics. The continuum limit in the form of a nonlocal PDE has been very successful for studying synchronization and pattern formation in large systems of coupled oscillators on a variety of graphs (Medvedev 2014c; Medvedev and Tang 2015; Medvedev and Tang 2020; Wiley et al. 2006). Therefore, it is important to understand the accuracy of approximation of large dynamical networks by a continuum equation. For solutions of initial value problems on convergent families of graphs, this was done in Medvedev (2014a,2014b; 2019).

In many theoretical studies as well as in practical applications, valuable information about system dynamics is gained by studying regimes bifurcating from simpler solutions under the variation of the control parameter. Therefore, it is of interest to understand how well and under what conditions, the bifurcation structure of large networks can be obtained from its continuum limit. Specifically, suppose the continuum model undergoes a bifurcation at a certain value of the control parameter. What can be said about the discrete system? Will it undergo a bifurcation at a close parameter value? Will the bifurcating solutions resemble those obtained in the continuum case? These are nontrivial questions in general, because certain features (such as symmetries) that are present in the continuum limit may not survive discretization. The questions become even more challenging if the large network system is random.

In this paper, following the work of Bramburger and Holzer (2023), we address these questions in the context of the Turing bifurcation in the discrete Swift–Hohenberg equation (SHE) on deterministic (Cayley) and random graphs. We postpone the discussion of how our approach and results differ from Bramburger and Holzer (2023) and turn next to the formulation of the discrete and continuous models for the Turing bifurcation.

Turing bifurcation is a well-known pattern formation mechanism named after the work of Turing on morphogenesis (Turing 1952). The mechanism is triggered by the instability of the spatially uniform state with respect to a periodic perturbation. As a result of instability, periodically modulated state is formed in the time evolution of the nonlinear model. Turing bifurcation on networks has been studied in many physics publications, e.g., (Asllani et al. 2014; Hütt et al. 2022; Kouvaris et al. 2015; Nakao and Mikhailov 2010; Wolfrum 2012).

The classical SHE plays a prominent role in the theory of pattern formation (see Collet and Eckmann (1990) and references therein). It has the following form

$$\partial_t u = -\left(1 + \partial_x^2\right)^2 u + \gamma u - u^3, \quad x \in \mathbb{T} \doteq \mathbb{R}/\mathbb{Z}, \tag{1.1}$$

where $u(t, x) \in \mathbb{R}$ and γ is a control parameter. The normal form reduction near the bifurcation, which makes use of the symmetries present in the system, shows existence

of a two-parameter family of stable stationary nontrivial solutions bifurcating from the trivial solution $u \equiv 0$ (see Section 2.4.3 in Haragus and Iooss (2011)):

$$u_{\gamma,\delta}(x) = 2\sqrt{\frac{\gamma}{3}}\cos(x+\delta) + O(\gamma^{3/2}) \tag{1.2}$$

for small positive γ and every $\delta \in \mathbb{T}$.

The nonlocal SHE is obtained by replacing the second derivative ∂_x^2 with a nonlocal operator L_W:

$$\partial_t u = -(L_W - \kappa)^2 u + \gamma u - u^3, \quad x \in \mathbb{T}, \tag{1.3}$$

where

$$(L_W f)(x) = \int_{\mathbb{T}} W(x,y)\,[f(y) - f(x)]\,\mathrm{d}y =: (K_W f)(x) - d_W(x) f(x). \tag{1.4}$$

Here, $W : \mathbb{T}^2 \to [0,1]$ is a measurable function that is symmetric a.e. on $\mathbb{T}^2$, and $f \in L^1(\mathbb{T})$.

In this paper, we assume that W has the following form

$$W(x,y) = S(x-y) \tag{1.5}$$

for a given even function $S \in L^1(\mathbb{T})$. In this case, d_W is independent of $x \in \mathbb{T}$. Graphons of the form (1.5) arise as limits of convergent sequences of Cayley graphs. For this reason, they are referred to as **Cayley graphons** (cf. Ghandehari et al. (2022)). It is instructive to study this case first, because the nonlocal SHE (1.3) with (1.4) and (1.5) is the closest nonlocal analog of the classical model (1.1) on a periodic domain. Since K_W has a discrete (real) spectrum with the only accumulation point at zero, the bifurcation of stable stationary nontrivial solutions occurs if κ is set to

$$\kappa = -d_W + \lambda_{k_0}, \quad k_0 \in \mathbb{N},$$

where $\{\lambda_k\}_{k\in\mathbb{Z}}$ are eigenvalues of K_W satisfying $\lambda_{-k} = \lambda_k$, $k \in \mathbb{N}$. Similar to (1.2), we are interested in solutions bifurcating from $u = 0$ for small γ. The normal form analysis of (1.3) closely resembles the normal form analysis of (1.1) and illustrates the role of translation invariance in the continuum model, see Theorem 3.8 below.

Along with the nonlocal model (1.3), we consider a discrete model on a graph Γ given by

$$\dot{u} = -(L_\Gamma - \kappa)^2 u + \gamma u - u^3, \tag{1.6}$$

where $u(t) \in \mathbb{R}^n$, the cubic nonlinearity u^3 is understood in the componentwise sense, and the graph Laplacian L_Γ is defined as follows

$$(L_\Gamma u)_i = \frac{1}{n}\sum_{j=1}^{n} a_{ij}\left(u_j - u_i\right), \tag{1.7}$$

which is associated with the adjacency matrix $A_\Gamma = (a_{ij})_{1\le i,j\le n}$.

In this paper, we study (1.6) with (1.7) on two families of graphs, one is deterministic and the other is random. Both families are constructed using a given W and converge to W almost surely. We refer the reader to Medvedev (2014a, 2019) for the overview of the ideas from the graph limit theory that are relevant here and to the references in the literature on this subject. For either graph model, one can show that the solution of the IVP for (1.3) approximates the solutions of the IVPs for (1.6) on finite time intervals (cf. Medvedev (2014a, b, 2019)). Thus, (1.3) provides a common continuum limit for the discrete models on both deterministic and random graphs. Note that this however does not guarantee that the solutions bifurcating from the trivial solution will resemble (1.2). In fact, in general, it is not clear that the discrete models will undergo a bifurcation at all. The reason for this is that the translation symmetry present in the continuum model does not survive discretization. The lack of the translation symmetry affects computations of the normal forms and thus the bifurcations. Our analysis predicts the exact number of solution families bifurcating from the trivial solution in the deterministic model, see Theorem 4.2, based on the discrete group of symmetries. On the other hand, the symmetries are broken in the random model and we are only able to find the lower and upper bounds on the number of solution families bifurcating from the trivial solution, see Theorem 5.1.

The organization of the paper is as follows. In Sect. 2, we complete the description of the discrete model (1.6) with (1.7) by providing the details on the deterministic and random graphs. The former are weighted Cayley graphs and the latter are W-random graphs (cf. Lovász and Szegedy (2006)).

After that we turn to the analysis of the continuous model in Sect. 3. Specifically, we demonstrate the well-posedness of the continuous model and analyze the bifurcation of the spatially homogeneous solutions. The bifurcation analysis is based on the normal form of the system in the Fourier coordinates. The derivation of the normal form uses the symmetries present in the system and resembles the analysis of the classical SHE in Haragus and Iooss (2011). The existence of a family of spatially periodic solutions is invariant with respect to the continuous spatial translations.

In Sect. 4, we study discrete SHE on weighted Cayley graphs. The bifurcation analysis follows the same lines as in the continuous case, where in place of Fourier transform we now use the discrete Fourier transform. An important distinction of the discrete model is that the invariance under any translations in the continuous system is replaced by the invariance with respect to a discrete group of translations. This results in finitely many solutions bifurcating from the trivial solution instead of the continuous family (1.2).

In Sect. 5, we move on to study the discrete model on random graphs, which is the main problem addressed in this paper. In the random setting, the discrete model does not possess the discrete translational invariance and the normal form approach, which worked for Cayley graphs, is no longer applicable. To overcome this obstacle, we use the proximity of the system on a sufficiently large random graph to that analyzed in Sect. 4 to derive a leading order approximation for the normal form. This allows us to study the bifurcation for the system on random graphs and to obtain precise bounds on the number of solution families bifurcating in each random realization of the discrete graph. This is where our approach is different from the approach taken in Bramburger and Holzer (2023). The normal form for the bifurcation on a random

graph is compared with the one on the associated discrete deterministic graph instead of the one on the associated continuous nonlocal model. We determine the translational parameter precisely from the normal form, whereas the translational parameter is defined implicitly in (Bramburger and Holzer 2023, Theorem 4.1) from a linear transformation of eigenvectors of the linearized equations. Additional comments on the differences between our work and Bramburger and Holzer (2023) can be found in Remark 5.7.

In Sect. 6, we present numerical experiments with SHE on small-world graphs. This example illustrates the selection of random stationary patterns in SHE on random graphs. We also explain the implications of the lack of continuous translational symmetry in the corresponding averaged SHE on deterministic Cayley graph. In Sect. 7, we discuss the utility of graphons in the analysis of dynamical systems on graphs and potential applications of our techniques to related network models.

The approximation result needed for the analysis of SHE on random graphs is given in Appendix. It is derived using the method of Guédon and Vershynin (2016) based on the concentration inequality for adjacency matrices of W-random graphs.

2 Discretization

The goal of this section is to complete the formulation of the discrete model (1.6) by supplying the details on the families of deterministic and random graphs. In what follows, we assume that n is even in (1.6) and denote $N = n/2$. This assumption is used to simplify computations of the normal forms. We will denote the deterministic graph by Γ_W^N and the random graph by $\tilde{\Gamma}_W^N$.

2.1 The Discrete SHE on Deterministic Graphs

To define the family of deterministic graphs (Γ_W^N), we fix $N \in \mathbb{N}$ and discretize $\mathbb{T}$ as follows. Let $h \doteq \frac{1}{2N}$, $x_i = ih$, and

$$Q_i = \left[x_i - \frac{h}{2}, x_i + \frac{h}{2}\right), \quad i \in [-N+1, N-1],$$
$$Q_N = \left[\frac{-1}{2}, \frac{-1}{2} + \frac{h}{2}\right) \bigcup \left[\frac{1}{2} - \frac{h}{2}, \frac{1}{2}\right).$$

Γ_W^N is a weighted graph on $2N$ nodes indexed by integers from $[-N+1, N]$. An edge between nodes i and j is supplied with a weight

$$a_{ij} = a_{ji} = (2N)^2 \int_{Q_i} \int_{Q_j} W(x, y)\mathrm{d}x\mathrm{d}y \qquad -N+1 \le i < j \le N.$$

In addition, we assume $a_{ii} = 0,\ i \in [-N+1, N]$.

Since $W(x, y) = S(x - y)$ according to (1.5), we have a Toeplitz matrix $A = (a_{ij})$ with

$$\begin{aligned} a_{i+k\,j+k} &= (2N)^2 \int_{Q_{i+k}} \int_{Q_{j+k}} S(x-y)\mathrm{d}x\mathrm{d}y \\ &= (2N)^2 \int_{Q_i} \int_{Q_j} S(x-y)\mathrm{d}x\mathrm{d}y = a_{ij}. \end{aligned} \tag{2.1}$$

If $S_k := a_{k0}$, then $a_{ij} = S_{i-j}$ and the graph Laplacian on Γ_W^N can be rewritten in the form:

$$\begin{aligned} (L_W^N u)_i &= \frac{1}{2N} \sum_{j=-N+1}^{N} S_{i-j}\left(u_j - u_i\right) \\ &= \frac{1}{2N} \sum_{j=-N+1}^{N} S_{i-j} u_j - \left(\frac{1}{2N} \sum_{j=-N+1}^{N} S_{i-j}\right) u_i \\ &=: \left(A_W^N u\right)_i - d_W^N u_i, \end{aligned} \tag{2.2}$$

where d_W^N is a constant independent of i. The SHE on the deterministic graph Γ_W^N has the following form:

$$\dot{u} = -\left(L_W^N - \kappa\right)^2 u + \gamma u - u^3, \tag{2.3}$$

where L_W^N is defined in (2.2).

2.2 The Discrete SHE on Random Graphs

The second family of graphs $(\tilde{\Gamma}_W^N)$ is random and corresponds to Γ_W^N, $N \in \mathbb{N}$. Denote the adjacency matrix of $\tilde{\Gamma}_W^N$ by $\tilde{A}^N = (\tilde{a}_{ij})_{-N+1 \le i,j \le N}$. We postulate that two distinct nodes of $\tilde{\Gamma}_W^N$ i and j are connected with probability a_{ij}, i.e.,

$$\mathbb{P}(\tilde{a}_{ij} = 1) = a_{ij}, \quad \mathbb{P}(\tilde{a}_{ij} = 0) = 1 - a_{ij}. \tag{2.4}$$

In addition, $\tilde{a}_{ii} = 0$ and $\tilde{a}_{ji} = \tilde{a}_{ij}$. The SHE on the random graph $\tilde{\Gamma}_W^N$ is given in the form:

$$\dot{u} = -\left(\tilde{L}_W^N - \kappa\right)^2 u + \gamma u - u^3, \tag{2.5}$$

where

$$(\tilde{L}_W^N u)_i = \frac{1}{N} \sum_{j=1}^{N} \tilde{a}_{ij}\left(u_j - u_i\right) = \left(\tilde{A}_W^N u\right)_i - (\tilde{D}_W^N u)_i, \tag{2.6}$$

where $\tilde{D}_W^N$ is a diagonal matrix.

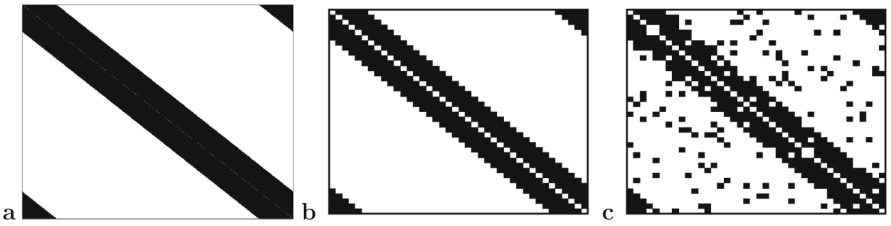

Fig. 1 **a** W takes values $1-p$ and p over the black and white regions, respectively. **b, c** Pixel plots of the adjacency matrix of Γ_W^N and its random counterpart $\tilde{\Gamma}_W^N$

Graphs defined by (2.4) are dense almost surely. In dense graphs the number of edges scales quadratically with the number of vertices, i.e., under this model Γ_W^N has $\mathcal{O}(N^2)$ edges. In this paper, we extend the random graph model to allow for sparse graphs. To this end, we introduce a nonincreasing sequence $\varsigma_N \in (0, 1]$ and modify (2.4) as follows

$$\mathbb{P}(\tilde{a}_{ij} = \varsigma_N^{-1}) = \varsigma_N a_{ij}, \quad \mathbb{P}(\tilde{a}_{ij} = 0) = 1 - \varsigma_N a_{ij}. \tag{2.7}$$

As before, $\tilde{a}_{ii} = 0$ and $\tilde{a}_{ji} = \tilde{a}_{ij}$.

If $\varsigma_N \equiv 1$ then (2.7) reduces to (2.4) and we obtain the sequence of dense random graphs as above. On the other hand, if $\varsigma_N \searrow 0$ then the expected number of edges in $\tilde{\Gamma}_W^N$ is $N(N-1)\varsigma_N \ll N^2$, which implies that $\tilde{\Gamma}_W^N$ is a sparse graph with probability 1. By varying the rate of convergence of ς_N to zero, one can control the degree of sparseness of $\tilde{\Gamma}_W^N$. We need to impose the following technical condition on (ς_N):

$$1 \geq \varsigma_N \geq MN^{-1/3}, \tag{2.8}$$

for some $M > 0$ independent of N. Assumption (2.8) is needed to control the deviation of the adjacency and degree matrices for the random graph model from their expected values (see (A.6) and Remark A.3).

We illustrate the families of graphs, which we just defined, with the following example.

Example 2.1 Fix $p \in [0, 1]$, $r \in (0, \frac{1}{2})$, and define an even function $S \in L^1(\mathbb{T})$ in the form:

$$S(x) = \begin{cases} 1-p, & |x| \leq r, \\ p, & r < |x| \leq \frac{1}{2}. \end{cases}$$

If $p = 0$ Γ_W^N is very close to the Cayley graph on $\mathbb{Z}_{2N}$ with the set of generators given by $\{\pm 1, \pm 2, \ldots, \pm\lfloor 2Nr \rfloor\}$. For $p \in (0, \frac{1}{2})$, $\tilde{\Gamma}_W^N$ is a small-world graph (Watts and Strogatz 1998). Figure 1 illustrates the example with $W(x, y) = S(x - y)$.

Remark 2.2 The W-random graph interpretation of the small-world network (2.4) used in this paper was introduced in Medvedev (2014b). A slightly different model was considered in Bramburger and Holzer (2023).

Remark 2.3 The deterministic SHE model (2.3) is a Galerkin approximation of the continuous SHE model (1.3). On the other hand, it is also related to the random model (2.5) via averaging, because $\mathbb{E}\tilde{a}_{ij} = a_{ij}$ by construction. Therefore, one can view the continuous SHE model (1.3) as a continuum limit of either of the discrete models (2.3) or (2.5). For a related class of nonlocal models, it is known that the initial-value problems for the deterministic and random discrete models approximate that for the continuum one (Medvedev 2014a, 2019). The same techniques apply to the models at hand and the approximation results continue to hold for the discrete and continuum SHEs. However, the analysis in the remainder of this paper does not depend on the validity of these results.

3 The Continuum SHE

In this section, we study the nonlocal SHE model (1.3), which serves as a continuum limit for the discrete SHE models (2.3) and (2.5) on deterministic and random graphs Γ_W^N and $\tilde{\Gamma}_W^N$, respectively. Our objective is to obtain a spatially dependent steady state via a Turing bifurcation of the trivial solution. For W in the form (1.5), the nonlocal SHE on Cayley graphon can be written in the form

$$\partial_t u = -\left(K_S - d_S - \kappa\right)^2 u + \gamma u - u^3, \tag{3.1}$$

where κ and γ are real parameters and

$$(K_S f)(x) = \int_{\mathbb{T}} S(x-y) f(y) \mathrm{d}y, \tag{3.2}$$

$$d_S = \int_{\mathbb{T}} S(x) \mathrm{d}x. \tag{3.3}$$

Throughout this section, we assume that S is a given integrable function on $\mathbb{T}$, i.e., $S \in L^1(\mathbb{T})$. Furthermore, S is assumed to be even almost everywhere. By Young's convolution inequality, K_S is a bounded operator from $L^p(\mathbb{T})$ to $L^p(\mathbb{T})$ for any $1 \leq p \leq \infty$ with the bound

$$\|K_S f\|_{L^p(\mathbb{T})} \leq \|S\|_{L^1(\mathbb{T})} \|f\|_{L^p(\mathbb{T})}. \tag{3.4}$$

Remark 3.1 Since K_S is a bounded operator from $L^2(\mathbb{T})$ to $L^2(\mathbb{T})$ and $\mathbb{T}$ is compact, the spectrum $\sigma(L_S)$ is purely discrete and consists of eigenvalues $\{\lambda_k\}_{k\in\mathbb{Z}}$ obtained from the Fourier modes:

$$\lambda_k = \int_{\mathbb{T}} S(x) e^{-2\pi i k x} \mathrm{d}x, \quad k \in \mathbb{Z}.$$

Since S is an even function,

$$\sigma(K_S) = \{\lambda_0,\ \lambda_1 = \lambda_{-1},\ \lambda_2 = \lambda_{-2},\ \cdots\}$$

consists of real eigenvalues. However, unless S is even on $\mathbb{T}$, K_S is not a self-adjoint operator in $L^2(\mathbb{T})$ and the eigenvalues $\{\lambda_k\}_{k\in\mathbb{Z}}$ only satisfy the relation $\lambda_k = \bar{\lambda}_{-k}$ for $k \in \mathbb{N}$ which does not exclude the possibility of complex eigenvalues.

The following lemma gives the well-posedness result of the time-evolution problem (3.1) in the phase space $\mathcal{X} := L^\infty(\mathbb{T})$, which is continuously embedded into $L^2(\mathbb{T})$ due to the bound $\|f\|_{L^2(\mathbb{T})} \leq \|f\|_{L^\infty(\mathbb{T})}$.

Lemma 3.2 *Assume that $S \in L^1(\mathbb{T})$ and its periodic extension to $\mathbb{R}$ is an even function. For every $u_0 \in \mathcal{X}$, there exists a unique global solution $u \in C^1([0,\infty),\mathcal{X})$ such that $u(0,\cdot) = u_0$. The unique solution $u \in C^1([0,\tau_0],\mathcal{X})$ is Lipschitz continuous with respect to $u_0 \in \mathcal{X}$ for every finite $\tau_0 > 0$.*

Proof By (3.4) with $p = \infty$, K_S is a bounded operator from $\mathcal{X}$ to $\mathcal{X}$. In addition, the nonlinear term of (3.1) is closed in $\mathcal{X}$ due to the bound $\|f^3\|_{L^\infty} \leq \|f\|_{L^\infty}^3$. Hence the vector field

$$A(u) \doteq -(K_S - d_S - \kappa)^2 u + \gamma u - u^3$$

is a C^1 map from $\mathcal{X}$ to $\mathcal{X}$. By the standard results of the semi-group theory (Cazenave and Haraux 1998, Chapter 3), for every $u_0 \in \mathcal{X}$, there exists a unique local solution $u \in C^1([0,\tau_0],\mathcal{X})$ for some $\tau_0 > 0$. Thanks to the repulsive cubic nonlinearity, we have

$$\begin{aligned} u \geq 0: &\quad \partial_t |u| \leq -(K_S - d_S - \kappa)^2 u + \gamma u, \\ u \leq 0: &\quad \partial_t |u| \leq (K_S - d_S - \kappa)^2 u - \gamma u, \end{aligned}$$

which together yields the following bound:

$$\begin{aligned} \frac{d}{dt}\|u(t,\cdot)\|_{L^\infty(\mathbb{T})} &\leq \|(K_S - d_S - \kappa)^2 u\|_{L^\infty(\mathbb{T})} + \gamma \|u(t,\cdot)\|_{L^\infty(\mathbb{T})} \\ &\leq \left[(\|S\|_{L^1(\mathbb{T})} + |\kappa| + |d_S|)^2 + |\gamma| \right] \|u(t,\cdot)\|_{L^\infty(\mathbb{T})}. \end{aligned}$$

Hence, the L^∞-norm of the local solution $u(t,\cdot)$ cannot blow up in a finite time $t \in [0,\tau_0]$ and the local solution $u \in C^1([0,\tau_0],\mathcal{X})$ is extended to the infinite time as $u \in C^1([0,\infty),\mathcal{X})$. Lipschitz continuity of the local solution $u \in C^1([0,\tau_0],\mathcal{X})$ with respect to $u_0 \in \mathcal{X}$ for every finite $\tau_0 > 0$ follows from Gronwall's inequality. □

Remark 3.3 The nonlinear term of (3.1) is not closed in $L^2(\mathbb{T})$. However, it is closed in $H^1_{\rm per}(\mathbb{T})$ given by

$$H^1_{\rm per}(\mathbb{T}) \doteq \left\{ f \in L^2(\mathbb{T}) : \quad f' \in L^2(\mathbb{T}) \right\},$$

since $H^1_{\rm per}(\mathbb{T})$ is a Banach algebra with respect to pointwise multiplication. Moreover, $H^1_{\rm per}(\mathbb{T})$ is continuously embedded into a space of bounded and continuous functions

satisfying the periodic boundary conditions. Compared to $H^1_{\rm per}(\mathbb{T})$, functions in the phase space $\mathcal{X} = L^\infty(\mathbb{T})$ do not have to be continuous or to satisfy the periodic boundary conditions. This is more suitable in the context of solutions of the discrete SHE on deterministic and random graphs.

Lemma 3.4 *If $u(t,x)$ is a solution of (3.1), so are $u(t,x+h)$, $u(t,-x)$, and $-u(t,x)$.*

Proof The continuous SHE (3.1) admits the following symmetries:

- the spatial translation $x \mapsto x+h$, $\forall h \in \mathbb{R}$ due to periodic conditions,
- the spatial reflection $x \mapsto -x$ due to even S,
- the sign reflection $u \mapsto -u$ due to odd nonlinearity,

which can be easily confirmed. The new solutions are generated by the symmetries. □

Remark 3.5 The nonlocal SHE (3.1) has two real parameters γ and κ. Parameter γ is small and is used to characterize Turing bifurcation of a spatially dependent steady state from the zero solution. On the other hand, parameter κ is the tuning parameter defined by the bifurcation condition according to the following definition.

Assumption 3.6 We fix $k_0 \in \mathbb{N}$, assume that $\lambda_k \neq \lambda_{k_0}$ for every $k \in \mathbb{N}\backslash\{k_0\}$, and choose $\kappa := \lambda_{k_0} - d_S = \lambda_{-k_0} - d_S$.

Remark 3.7 Since K_S is a compact operator on $L^2(\mathbb{T})$, eigenvalues $\{\lambda_n\}_{n\in\mathbb{Z}}$ satisfy $\lambda_n \to 0$ as $|n| \to \infty$. Hence, Assumption 3.6 implies that there is $C_0 > 0$ such that

$$|\lambda_k - \lambda_{k_0}| \geq C_0 \quad \text{for all } k \in \mathbb{N}, \quad k \neq k_0. \tag{3.5}$$

The following theorem presents the main result of this section. Although it is an exercise from (Haragus and Iooss 2011, Section 2.4.3), we write the computational details explicitly, since they are useful for analysis of Turing bifurcation in the discrete SHE.

Theorem 3.8 *Under Assumption 3.6, there exists $\gamma_0 > 0$ and $C_0 > 0$ such that for every $\gamma \in (0,\gamma_0)$ there exists a nontrivial time-independent solution $u_\gamma(\cdot+\delta)$ in $\mathcal{X}$ of the nonlocal SHE model (3.1), where u_γ is an even function satisfying*

$$\sup_{x\in\mathbb{T}} \left| u_\gamma(x) - \frac{2\sqrt{\gamma}}{\sqrt{3}} \cos(2\pi k_0 x) \right| \leq C_0 \sqrt{\gamma^3}, \tag{3.6}$$

and $\delta \in \mathbb{T}$ is an arbitrary translational parameter. The orbit of time-independent solutions $\{u_\gamma(\cdot+\delta)\}_{\delta\in\mathbb{T}}$ is asymptotically stable in the time evolution of the nonlocal SHE in $\mathcal{X}$.

Proof In order to use the center manifold theorem and to derive slow dynamics along the center manifold, we use the Fourier series

$$u(t,x) = \sum_{k\in\mathbb{Z}} a_k(t) e^{2\pi i k x}$$

and obtain the evolution problem in the form

$$\dot{a}_k = -(\lambda_k - \lambda_{k_0})^2 a_k + \gamma a_k - \sum_{k_1,k_2\in\mathbb{Z}} a_{k_1} a_{k_2} a_{k-k_1-k_2}, \tag{3.7}$$

where we have used that $\kappa = \lambda_{k_0} - d_S$. By standard results from Fourier analysis, $u(t,\cdot) \in \mathcal{X} = L^\infty(\mathbb{T})$ if $\{a_k(t)\}_{k\in\mathbb{Z}} \in \hat{\mathcal{X}} = \ell^1(\mathbb{Z})$ for every $t \geq 0$. The nonlinear term of (3.7) is closed, since $\ell^1(\mathbb{Z})$ is a Banach algebra with respect to the convolution sum.

Since u is real, we have $a_{-k} = \bar{a}_k$ for all $k \in \mathbb{Z}$. Due to the three symmetries identified in Lemma 3.4, the vector field in (3.7) is equivariant under the transformation

$$a_k \to a_k e^{2\pi i k h}, \quad k \in \mathbb{Z}, \quad h \in \mathbb{R}, \tag{3.8}$$

and under the transformations: $a_k \to a_{-k}$ and $a_k \to -a_k$. Consequently, the system (3.7) is closed on the subspaces

$$\hat{\mathcal{X}}_{\text{sym}} := \{\{a_k\}_{k\in\mathbb{Z}} \in \ell^1(\mathbb{Z},\mathbb{R}) : \ a_{-k} = a_k \ \} \tag{3.9}$$

and

$$\hat{\mathcal{X}}_{\text{bif}} := \{\{a_k\}_{k\in\mathbb{Z}} \in \ell^1(\mathbb{Z},\mathbb{C}) : \ a_{-k} = a_k = 0, \ k \neq mk_0, \ m \in \{1,3,5,\cdots\}\}, \tag{3.10}$$

where $k_0 \in \mathbb{N}$ is defined in Assumption 3.6.

By Assumption 3.6, the rest of eigenvalues $\{\lambda_k\}_{k\in\mathbb{Z}\setminus\{\pm k_0\}}$ are bounded away from $\lambda_{k_0} = \lambda_{-k_0}$ with the bound (3.5). By the center manifold theorem (Haragus and Iooss 2011, Theorem 2.9), there exists a center manifold in $\hat{\mathcal{X}}_{\text{bif}}$ spanned by $A := a_{k_0} \in \mathbb{C}$ and $\bar{A} := a_{-k_0}$. Since the system is closed on (3.10), the center manifold can be expressed as graphs of functions:

$$a_{mk_0} = \Psi_m(A,\bar{A}), \quad a_{-mk_0} = \bar{\Psi}_m(A,\bar{A}), \quad m \in \{3,5,\cdots\}.$$

The dynamics on the center manifold can be expressed by the amplitude equations

$$\dot{A} = F_1(A,\bar{A}), \quad \dot{\bar{A}} = \overline{F_1(A,\bar{A})},$$

where F_1 is a C^∞ function in A and $\bar{A}$ with γ-dependent coefficients which commutes with the symmetries of (3.7). Due to the equivariance (3.8), the amplitude equations can be transformed to the normal form:

$$\dot{A} = A P_1(|A|^2), \tag{3.11}$$

where P_1 is a C^∞ function in $|A|^2$ with γ-dependent coefficients. Moreover, due to the symmetry with respect to the transformation $a_k \to a_{-k}$, P_1 has real-valued coefficients. Similarly, we express functions Ψ_m in the form:

$$\Psi_m(A, \bar{A}) = A^m P_m(|A|^2), \quad m \in \{3, 5, \cdots\}, \tag{3.12}$$

where P_m is a C^∞ function in $|A|^2$ with γ-dependent real-valued coefficients.

Due to the cubic nonlinearity in (3.7), we obtain

$$\dot{A} = \left[\gamma - 3|A|^2 + \mathcal{O}(|A|^4)\right] A, \tag{3.13}$$

where the remainder terms of the order of $\mathcal{O}(|A|^4)$ is defined by Ψ_3 since Ψ_m with $m \geq 5$ give a higher-order contribution of $\mathcal{O}(|A|^6)$ to the normal form (3.13). It follows from (3.13) that there exists a time-independent solution of the form

$$A_{\gamma,\delta} := \frac{\sqrt{\gamma}}{\sqrt{3}} \left[1 + \mathcal{O}(\gamma)\right] e^{2\pi k_0 i \delta}, \tag{3.14}$$

where δ is an arbitrary parameter. This time-independent solution (3.14) yields a nontrivial time-independent solution of the nonlocal SHE (3.1) in $\mathcal{X}$ satisfying the expansion in (3.6). Since the system (3.7) is closed on (3.9), if $\delta = 0$, then $a_{-k_0} = a_{k_0} = A_{\gamma,\delta=0}$ is real and so are $a_{\pm m k_0}$ for every $m \in \{3, 5, \cdots\}$. This yields the even function $u_\gamma \in \mathcal{X}$. Due to the translational symmetry (3.8), the parameter δ is equivalent to the translation of the solution $u_\gamma(\cdot + \delta)$.

To determine stability of the time-independent solution $u_\gamma(\cdot + \delta)$ for every given $\delta \in \mathbb{R}$, we note that all eigenvalues in the spectrum of $-(K_S - d_S - \kappa)^2$ are located in the left-half plane of the complex plane with the exception of the double zero eigenvalue. Hence, there is no unstable manifold of the system (3.7). The time-independent solution (3.14) is orbitally asymptotically stable in the time evolution of the reduced equation (3.11). By the standard decomposition near the orbit $\{u_\gamma(\cdot + \delta)\}_{\delta \in \mathbb{T}}$, a perturbation of the initial solution $u_\gamma(\cdot + \delta_0)$ defines a time-dependent solution which approaches as $t \to +\infty$ exponentially fast to the final solution $u_\gamma(\cdot + \delta_\infty)$ with δ_∞ being close to δ_0. Hence, the orbit $\{u_\gamma(\cdot + \delta)\}_{\delta \in \mathbb{T}}$ is asymptotically stable in the time evolution of the nonlocal SHE in $\mathcal{X}$. □

Remark 3.9 The leading-order approximation for Ψ_3 in (3.12) can be obtained from (3.7) and (3.13). Substitution yields

$$\begin{aligned}
&[\gamma - 3|A|^2 + \mathcal{O}(|A|^4)]\left[3P_3(|A|^2) + |A|^2 P_3'(|A|^2)\right] \\
&= \left[\gamma - (\lambda_{3k_0} - \lambda_{k_0})^2\right] P_3(|A|^2) - 1 + \mathcal{O}(|A|^2),
\end{aligned}$$

which is solved by expanding $P_3(|A|^2)$ in $|A|^2$ with the leading order:

$$P_3(|A|^2) = \frac{-1}{(\lambda_{3k_0} - \lambda_{k_0})^2 + 2\gamma} + \mathcal{O}(|A|^2), \tag{3.15}$$

where $\lambda_{3k_0} \neq \lambda_{k_0}$ by the assumption. Similarly, one can find the leading-order expansions of Ψ_m in (3.12) for $m \geq 5$.

Related to the time-independent solution $u_\gamma(\cdot+\delta)$ of the nonlocal SHE in Theorem 3.8, we can introduce the linearized operator in the form

$$\mathcal{L}_\gamma := -(K_S - \lambda_{k_0})^2 + \gamma - 3u_\gamma^2, \tag{3.16}$$

where we have used that $\kappa = \lambda_{k_0} - d_S$ according to Assumption 3.6. Since u_γ is a bounded function on $\mathbb{T}$, $\mathcal{L}_\gamma$ is a bounded operator from $L^2(\mathbb{T})$ to $L^2(\mathbb{T})$ for all sufficiently small γ for which u_γ is defined. Hence, the spectrum of $\mathcal{L}_\gamma$ is purely discrete and consists of real eigenvalues, see Remark 3.1. The following lemma uses the smallness of γ and gives a precise information on the location of these eigenvalues.

Lemma 3.10 *Let $u_\gamma \in \mathcal{X}$ be defined by Theorem 3.8 for $\gamma \in (0, \gamma_0)$ and assume that $u_\gamma' \in L^2(\mathbb{T})$. The spectrum of $\mathcal{L}_\gamma$ given by (3.16) in $L^2(\mathbb{T})$ consists of eigenvalues ordered as $\{\Lambda_k(\gamma)\}_{k\in\mathbb{N}}$ such that $\Lambda_1(\gamma) = 0$ and $\Lambda_k(\gamma) < 0$, $k \geq 2$ satisfy*

$$|\Lambda_2(\gamma)| \leq C_1\gamma, \quad |\Lambda_k(\gamma)| \geq C_2, \quad k \geq 3$$

where C_1, C_2 are γ-independent positive constants.

Proof The existence of $\Lambda_1(\gamma) = 0$ follows from the translational invariance of the nonlocal SHE given by (3.1) since $\delta \in \mathbb{R}$ is a free parameter of the steady state $u_\gamma(\cdot+\gamma) \in \mathcal{X}$ in Theorem 3.8. Since $u_\gamma' \in L^2(\mathbb{T})$ is assumed, we obtain by direct differentiation that

$$\mathcal{L}_\gamma u_\gamma'(\cdot+\delta) = 0,$$

so that $\Lambda_1(\gamma) = 0$ for $\gamma \in (0, \gamma_0)$.

The rest of the spectrum of $\mathcal{L}_\gamma$ in $L^2(\mathbb{T})$ follows from the perturbation theory for self-adjoint operators with purely discrete spectrum which implies continuity of eigenvalues with respect to small parameter $\gamma \in (0, \gamma_0)$. The eigenvalue $\Lambda_2(\gamma)$ coincides with the linearization of the slow motion at the center manifold given by (3.13):

$$\begin{aligned}\Lambda_2(\gamma) &= \gamma - 9|A_{\gamma,\delta}|^2 + \mathcal{O}(|A_\gamma|^4) \\ &= -2\gamma + \mathcal{O}(\gamma^2),\end{aligned}$$

which is strictly negative with the bound $|\lambda_2(\gamma)| \leq C_1\gamma$ with some γ-independent constant $C_1 > 0$ for $\gamma \in (0, \gamma_0)$. Eigenvalues $\Lambda_k(\gamma)$ for $k \geq 3$ are γ-close to $-(\lambda_k - \lambda_{k_0})^2$ for $k \in \mathbb{Z}\backslash\{k_0, -k_0\}$ which are strictly negative and bounded away from 0 by Assumption 3.6. Hence, $|\Lambda_k(\gamma)| \geq C_2$ for all $k \geq 2$ with some γ-independent constant $C_2 > 0$ for $\gamma \in (0, \gamma_0)$. □

Remark 3.11 Due to the presence of zero eigenvalue $\Lambda_1(\gamma) = 0$, the operator $\mathcal{L}_\gamma$ is not invertible. This creates difficulties in the persistence argument when the limiting nonlocal model (3.1) is replaced by the discrete SHE models on the deterministic or random graphs, which destroy the continuous translational symmetry.

4 The Discrete SHE on Cayley Graphs

Here, we study the discrete SHE (2.3) on the deterministic Cayley graph Γ_W^N. By using (2.2), we rewrite the discrete model in the form:

$$\dot{u}_j = -[(A_W^N - d_W^N - \kappa)^2 u]_j + \gamma u_j - u_j^3, \quad j \in \mathbb{Z}_N := \mathbb{Z}/(2N\mathbb{Z}), \tag{4.1}$$

where N is integer, κ and γ are real parameters, and the linear operator $A_W^N : \mathbb{Z}_N \to \mathbb{Z}_N$ is given by the convolution sum

$$[A_W^N u]_j = \frac{1}{2N} \sum_{l \in \mathbb{Z}_N} S_{j-l} u_l, \quad j \in \mathbb{Z}_N, \tag{4.2}$$

where $\{S_j\}_{j \in \mathbb{Z}_N}$ satisfies $S_{-j} = S_j$ for all $j \in \mathbb{Z}_N$. System of differential equations (4.1) can be viewed as an evolution equation on $\mathbb{Z}_N$. The classical solutions are interpreted as elements of $C^1(\mathbb{R}, \mathbb{R}^{\mathbb{Z}_N})$, the space of continuously differentiable vector functions of $t \in \mathbb{R}$.

Lemma 4.1 *If $\{u_j(t)\}_{j \in \mathbb{Z}_N}$ is a solution of the discrete SHE (4.1), so are*

$$\{u_{j+m}(t)\}_{j \in \mathbb{Z}_N}, \quad \{u_{-j}(t)\}_{j \in \mathbb{Z}_N}, \quad \{u_{m-j}(t)\}_{j \in \mathbb{Z}_N}, \quad \text{and} \quad \{-u_j(t)\}_{j \in \mathbb{Z}_N}. \tag{4.3}$$

Proof Similarly to the continuous SHE (3.1), the discrete SHE (4.1) admits the following three symmetries:

- the discrete spatial translation $j \mapsto j + m, \forall m \in \mathbb{Z}_N$ due to periodic conditions,
- the spatial reflection $j \mapsto -j$ due to even $\{S_j\}_{j \in \mathbb{Z}_N}$,
- the sign reflection $u \mapsto -u$ due to odd nonlinearity,

which can be easily confirmed. The new solutions (4.3) are generated from $\{u_j(t)\}_{j \in \mathbb{Z}_N}$ by symmetries. □

Our objective is to obtain a spatially dependent steady state of the discrete SHE (4.1) via a Turing bifurcation of the zero solution. By using the discrete Fourier transform, one can obtain eigenvalues of A_W^N in the form $\{\lambda_k^N\}_{k \in \mathbb{Z}_N}$ with

$$\lambda_k^N = \frac{1}{2N} \sum_{j \in \mathbb{Z}_N} S_j e^{-\frac{i\pi kj}{N}}, \quad k \in \mathbb{Z}_N. \tag{4.4}$$

Since $S_{-j} = S_j$ for all $1 \le j \le N-1$, then $\lambda_k^N = \lambda_{-k}^N$ for $1 \le k \le N-1$. We again use parameter γ in (4.1) to characterize Turing bifurcation and parameter κ to satisfy the bifurcation condition.

We will locate a spatially dependent steady state bifurcating from the zero solution by adapting the proof of Theorem 3.8 with the discrete Fourier transform replacing Fourier series. One key new feature of the center manifold analysis is that the translational parameter $\delta \in \mathbb{T}$ which was arbitrary in Theorem 3.8 takes exactly $4N$

admissible values under some nondegeneracy conditions. In comparison with Assumption 3.6, we set $k_0 = 1$ for the bifurcating mode in order to simplify computations of the normal form. The following theorem presents the main result of this section.

Theorem 4.2 *Assume that $\lambda_k^N \neq \lambda_1^N$ for $k \neq \pm 1$ and choose $\kappa := \lambda_1^N - d_W^N = \lambda_{-1}^N - d_W^N$. If $r_N \neq 0$, where r_N is given by (4.15), then there exists $\gamma_0 > 0$ and $C_0 > 0$ such that for every $\gamma \in (0, \gamma_0)$ and every integer $N \geq 3$ there exist two nontrivial time-independent solutions $u_\gamma^N, v_\gamma^N \in \mathbb{R}^{\mathbb{Z}_N}$ of the discrete SHE (4.1), where u_γ^N is symmetric about $j = 0$ and satisfies*

$$\sup_{j \in \mathbb{Z}_N} \left| u_j - \frac{2}{\sqrt{3}} \sqrt{\gamma} \cos\left(\frac{\pi j}{N} \right) \right| \leq C_0 \sqrt{\gamma^3}. \tag{4.5}$$

and v_γ^G is symmetric about the mid-point between $j = 0$ and $j = 1$ and satisfies

$$\sup_{j \in \mathbb{Z}_N} \left| u_j - \frac{2}{\sqrt{3}} \sqrt{\gamma} \cos\left(\frac{\pi j}{N} - \frac{\pi}{2N} \right) \right| \leq C_0 \sqrt{\gamma^3}. \tag{4.6}$$

One of the two solutions is asymptotically stable in the time evolution of the discrete SHE in $C^1(\mathbb{R}, \mathbb{R}^{\mathbb{Z}_N})$ and the other one is unstable. These solutions generate $(2N)$ asymptotically stable and $(2N)$ unstable solutions on $\mathbb{Z}_N$ via the discrete group of spatial translations.

Proof We use the discrete Fourier transform

$$u_j = \sum_{k \in \mathbb{Z}_N} a_k(t) e^{\frac{i\pi kj}{N}}, \quad j \in \mathbb{Z}_N, \tag{4.7}$$

with real a_0, a_N, and possibly complex $a_{-k} = \bar{a}_k$ for $1 \leq k \leq N-1$. The Fourier amplitudes are extended periodically with the period $2N$ as the sequence $\{a_k\}_{k \in \mathbb{Z}_N}$. The discrete SHE (4.1) transforms to the evolution problem in the form

$$\begin{aligned} \dot{a}_k = &-(\lambda_k^N - \lambda_1^N)^2 a_k + \gamma a_k - \sum_{-N \leq k_1, k_2, k-k_1-k_2 \leq N-1} a_{k_1} a_{k_2} a_{k-k_1-k_2} \\ &- \sum_{-N \leq k_1, k_2, k+2N-k_1-k_2 \leq N-1} a_{k_1} a_{k_2} a_{k+2N-k_1-k_2} \\ &- \sum_{-N \leq k_1, k_2, k-2N-k_1-k_2 \leq N-1} a_{k_1} a_{k_2} a_{k-2N-k_1-k_2}, \end{aligned} \tag{4.8}$$

where the summation terms are adjusted due to the $(2N)$-periodicity of the Fourier modes in the Fourier space and we have used that $\kappa = \lambda_1^N - d_W^N$. Symmetries in Lemma 4.1 imply that the system (4.8) is equivariant under the transformation

$$a_k \to a_k e^{\frac{i\pi km}{N}}, \quad k, m \in \mathbb{Z}_N \tag{4.9}$$

and under the transformations: $a_k \to a_{-k}$ and $a_k \to -a_k$. In particular, the system (4.9) is closed on the subspaces

$$\{a \in \mathbb{R}^{\mathbb{Z}_N} : \ a_{-k} = a_k, \ \ 1 \le k \le N-1\} \tag{4.10}$$

and

$$\{a \in \mathbb{C}^{\mathbb{Z}_N} : \ a_{-k} = a_k = 0, \ \text{for } k \ne m, \ m \in \{1, 3, 5, \ldots, M\}\}, \tag{4.11}$$

where $M = N$ if N is odd or $M = N-1$ if N is even.

We apply the center manifold theorem (Haragus and Iooss (2011), Theorem 2.9) under the assumption that $\lambda_k^N \ne \lambda_1^N$ for $k \ne \pm 1$. Similar to the proof of Theorem 3.8, there exists a center manifold of the system (4.8) spanned by $a_1 \equiv A \in \mathbb{C}$ and $a_{-1} = \bar{A}$. Since the system is closed on (4.11), the center manifold can be expressed as graphs of functions:

$$a_m = \Psi_m(A, \bar{A}), \quad a_{-m} = \bar{\Psi}_m(A, \bar{A}), \quad m \in \{3, 5, \ldots, M\}. \tag{4.12}$$

The slow dynamics on the center manifold can be expressed by the amplitude equations

$$\dot{A} = F_1(A, \bar{A}), \quad \dot{\bar{A}} = \overline{F_1(A, \bar{A})},$$

where F_1 is a C^∞ function in A and $\bar{A}$ with γ-dependent coefficients which commutes with the symmetries of (4.8). Compared to the normal form for the amplitude equations in (3.11) and (3.12), the discrete Fourier modes are $(2N)$-periodic so that

$$\left[Ae^{\frac{i\pi kj}{N}}\right]^{2N+1} = A^{2N+1}e^{\frac{i\pi kj}{N}} \quad \text{and} \quad \left[\bar{A}e^{\frac{-i\pi kj}{N}}\right]^{2N-1} = \bar{A}^{2N-1}e^{\frac{i\pi kj}{N}}.$$

Following the classification of normal forms under the symmetry (4.9) in Chossat and Lauterbach (2000), we transform the amplitude equations to the normal form:

$$\dot{A} = AQ_1(|A|^2, A^{2N}, \bar{A}^{2N}) + \bar{A}^{2N-1}R_1(|A|^2, A^{2N}, \bar{A}^{2N}), \tag{4.13}$$

where Q_1 and R_1 are C^∞ functions in $|A|^2$, A^{2N}, and $\bar{A}^{2N}$ with γ-dependent coefficients. Due to the symmetry with respect to the transformation $a_k \to a_{-k}$, Q_1 and R_1 have real-valued coefficients. Similarly, we express functions Ψ_m in the form:

$$\Psi_m(A, \bar{A}) = A^m Q_m(|A|^2, A^{2N}, \bar{A}^{2N}) + \bar{A}^{2N-m}R_m(|A|^2, A^{2N}, \bar{A}^{2N}), \tag{4.14}$$

where Q_m and R_m are C^∞ functions in $|A|^2$, A^{2N}, and $\bar{A}^{2N}$ with γ-dependent real-valued coefficients.

We assume the following nondegeneracy condition:

$$r_N := R_1(0, 0, 0) \ne 0, \tag{4.15}$$

where r_N is a γ-dependent real-valued coefficient. Similarly to (3.13), we obtain from the cubic nonlinearity in (4.8) that

$$Q_1(|A|^2, A^{2N}, \bar{A}^{2N}) = \gamma - 3|A|^2 + \mathcal{O}(|A|^4),$$

if $N \geq 3$. By using the polar form $A = \rho e^{i\theta}$, we write

$$\begin{cases} \dot{\rho} = \rho[\gamma - 3\rho^2 + \mathcal{O}(\rho^4)] + \cos(2N\theta)\rho^{2N-1}[r_N + \mathcal{O}(\rho^2)], \\ \dot{\theta} = -\sin(2N\theta)\rho^{2N-2}[r_N + \mathcal{O}(\rho^2)]. \end{cases}$$

If $r_N \neq 0$, there exist two distinct time-independent solutions for $\theta = 0$ and $\theta = \frac{\pi}{2N}$ on interval $[0, \frac{\pi}{N})$. If $N \geq 3$, both solutions can still be expressed at the leading order in the form:

$$A_{\gamma,\delta} = \frac{\sqrt{\gamma}}{\sqrt{3}} \left[1 + \mathcal{O}(\gamma)\right] e^{\frac{i\pi\delta}{N}}, \tag{4.16}$$

with either $\delta = 0$ (which corresponds to $\theta = 0$) or $\delta = \frac{1}{2}$ (which corresponds to $\theta = \frac{\pi}{2N}$). For $\delta = 0$, we get the real solution $\{a_k\}_{k\in\mathbb{Z}_N}$ on the subspace (4.10) that corresponds to the solution u_γ^N of the discrete SHE (4.1) which is symmetric about $j = 0$ and satisfies (4.5). For $\delta = \frac{1}{2}$, we get a complex solution $\{a_k\}_{k\in\mathbb{Z}_N}$ that corresponds to the real solution v_γ^N of the discrete SHE (4.1) which satisfies (4.6). The leading order and hence the solution v_γ^N is symmetric about the mid-point between $j = 0$ and $j = 1$ due to the symmetry with respect to the transformation $u_j \to u_{1-j}$ in Lemma 4.1.

To obtain the stability conclusion for the time-independent solutions, we observe that all eigenvalues in the spectrum of $-(A_W^N - \lambda_1^N)^2$ are located in the left-half plane of the complex plane with the exception of the double zero eigenvalue. If $r_N \neq 0$, then linearization of the time-dependent equation (4.13) at the leading-order solution (4.16) for $N \geq 3$ yields for the perturbations (ρ_1, θ_1):

$$\begin{cases} \dot{\rho}_1 = -2\gamma\rho_1 + \mathcal{O}(\gamma^2), \\ \dot{\theta}_1 = \mp\left(\frac{\gamma}{3}\right)^{N-1}\left[r_N + \mathcal{O}(\gamma)\right]\theta_1, \end{cases} \tag{4.17}$$

where the upper sign corresponds to the solution u_γ^N and the lower sign corresponds to the solution v_γ^N. Dynamics of (4.17) in ρ_1 is asymptotically stable, whereas dynamics of (4.17) in θ_1 is either asymptotically stable or unstable. This yields the conclusion that one of the two solutions u_γ^N and v_γ^N is asymptotically stable in the time evolution of the discrete SHE and the other one is unstable.

The two solutions u_γ^N and v_γ^N generate $(4N)$ solutions by using the discrete group of translations $u_j \mapsto u_{j\pm m}$ for every $m \in \mathbb{Z}_N$ by Lemma 4.1. The stability of the translated solutions coincides with the stability of u_γ^N and v_γ^N. □

Remark 4.3 Since

$$\cos\left(\frac{\pi j}{N} - \frac{\pi}{N}\right) = -\cos\left(\frac{\pi j}{N}\right),$$

N of $(2N)$ states obtained from either (4.5) or (4.6) with the discrete group of translations are the sign reflections of the other N states, in accordance with the sign reflection symmetry in Lemma 4.1.

Remark 4.4 The graphons defined by the graphs Γ_W^N used the formulation of the discrete SHE (4.1) converge to W, the kernel used in the continuous SHE (3.1), in the cut-norm as $N \to \infty$ (cf. (A.6)). The cut-norm is equivalent to the $\infty \to 1$ norm defined in (A.5) (cf. Lovász (2012)). Thus, $\lambda_k^N \to \lambda_k$ for every fixed $k \in \mathbb{Z}$ (Szegedy (2011)). From this, we conclude that Assumption 3.6 with $k_0 = 1$ implies the corresponding assumption of Theorem 4.2, i.e., $\lambda_k^N \neq \lambda_1^N$, $k \neq \pm 1$ for sufficiently large N.

Remark 4.5 If the nondegeneracy condition (4.15) is not satisfied, one needs to expand functions Q_1 and R_1 in (4.13) to the higher orders and to obtain the higher-order nondegeneracy conditions. If it happens that $R_1 \equiv 0$ and $Q_1(|A|^2, A^{2N}, \bar{A}^{2N}) = P_1(|A|^2)$, then the time-independent solution (4.16) exists with arbitrary $\delta \in \mathbb{R}/\mathbb{Z}$. In this degenerate case, there exists a family of nontrivial time-independent solutions $u_{\gamma,\delta}^N \in \mathbb{R}^{\mathbb{Z}_N}$ of the discrete SHE (4.1) with arbitrary parameter $\delta \in [0, 1]$, where $u_{\gamma,\delta}$ satisfies

$$\sup_{-N \le j \le N} \left| u_j - \frac{2}{\sqrt{3}} \sqrt{\gamma} \cos\left(\frac{\pi j}{N} - \frac{\pi \delta}{2N}\right) \right| \le C_0 \sqrt{\gamma^3}. \tag{4.18}$$

The orbit of time-independent solutions $\{u_{\gamma,\delta}^N\}_{\delta \in \mathbb{R}/\mathbb{Z}}$ is asymptotically stable in the time evolution of the discrete SHE in $C^1(\mathbb{R}, \mathbb{R}^{\mathbb{Z}_N})$. Although such degenerate cases may exist in other discrete models, see, e.g., Hupkes et al. (2011), the explicit computations for the particular discrete SHE model (4.1) show that $r_N \neq 0$ for every $N \ge 3$.

Remark 4.6 Cases $N = 1$ and $N = 2$ are exceptional. In both cases, the discrete Fourier transform in the subspace (4.11) is given by the sum of two terms

$$u_j = A(t) e^{\frac{i\pi j}{N}} + \bar{A}(t) e^{-\frac{i\pi j}{N}}, \tag{4.19}$$

If $N = 1$, then A in (4.19) is real and satisfies

$$\dot{A} = \gamma A - 4A^3,$$

from which the stable nontrivial solutions at $A = \pm\sqrt{\gamma}/2$ exist in addition to the unstable solution $A = 0$ for $\gamma > 0$. If $N = 2$, then A in (4.19) is complex and satisfies

$$\dot{A} = \gamma A - 3|A|^2 A - \bar{A}^3.$$

Using the polar form $A = \rho e^{i\theta}$, this equation is reduced to the system

$$\begin{cases} \dot{\rho} = \gamma\rho - 3\rho^3 - \rho^3\cos(4\theta), \\ \dot{\theta} = \rho^2\sin(4\theta), \end{cases}$$

from which the two nontrivial time-independent solutions are given by

$$(\rho,\theta) = \left(\frac{\sqrt{\gamma}}{2}, 0\right) \quad \text{and} \quad (\rho,\theta) = \left(\frac{\sqrt{\gamma}}{\sqrt{2}}, \frac{\pi}{4}\right).$$

The linearization shows that the first solution is linearly unstable and the second solution is asymptotically stable.

The following two examples give details of computations of the center manifold reductions for $N = 3$ and $N = 4$, for which the discrete Fourier transform in the subspace (4.11) is given by the sum

$$u_j = A(t)e^{\frac{i\pi j}{N}} + \bar{A}(t)e^{-\frac{i\pi j}{N}} + B(t)e^{\frac{3i\pi j}{N}} + \bar{B}(t)e^{-\frac{3i\pi j}{N}}. \tag{4.20}$$

These details show that the nondegeneracy condition (4.15) is satisfied for $N = 3, 4$.

Example 4.7 If $N = 3$, then A is complex and B is real. The system (4.1) in the decomposition (4.20) is reduced to the system of two equations

$$\begin{cases} \dot{A} = \gamma A - 3|A|^2 A - 12B^2 A - 6\bar{A}^2 B, \\ \dot{B} = -(\lambda_3^N - \lambda_1^N)^2 B + \gamma B - \frac{1}{2}(A^3 + \bar{A}^3) - 6|A|^2 B - 4B^3. \end{cases}$$

We compute the center manifold reduction $B = \Psi_3(A, \bar{A})$ in powers of A according to (4.14) with real B by writing

$$\Psi_3(A,\bar{A}) = \frac{1}{2}(A^3 + \bar{A}^3)\left[c_0 + \mathcal{O}(|A|^2)\right],$$

where c_0 is a real coefficient that depends on γ. From the system of differential equations for A and B, we find at the cubic order that

$$c_0 = \frac{-1}{(\lambda_3^N - \lambda_1^N)^2 + 2\gamma},$$

which agrees with the expansion (3.15). Substituting $B = \Psi_3(A, \bar{A})$ into the first equation of the system, we obtain consistently with (4.13) that the slow dynamics of A is given by

$$\dot{A} = A\left[\gamma - 3|A|^2 + \mathcal{O}(|A|^4)\right] - 3c_0\bar{A}^5\left[1 + \mathcal{O}(|A|^2)\right].$$

Since $r_{N=3} = -3c_0 > 0$, the nondegeneracy condition (4.15) is satisfied.

Example 4.8 If $N = 4$, then both A and B are complex. The system (4.1) in the decomposition (4.20) is reduced to the system of two complex-valued equations

$$\begin{cases} \dot{A} = \gamma A - 3(|A|^2 + 2|B|^2)A - B^3 - 3(\bar{A}B + \bar{B}^2)\bar{A}, \\ \dot{B} = -(\lambda_3^N - \lambda_1^N)^2 B + \gamma B - A^3 - 3(2|A|^2 + |B|^2)B - 3(A\bar{B} + \bar{A}^2)\bar{B}. \end{cases}$$

We compute the center manifold reduction $B = \Psi_3(A, \bar{A})$ in powers of A according to (4.14) by writing

$$\Psi_3(A, \bar{A}) = A^3 \left[c_0 + c_1 |A|^2 + \mathcal{O}(|A|^4) \right] + \bar{A}^5 \left[b_0 + \mathcal{O}(|A|^2) \right],$$

where c_0, c_1, and b_0 are real coefficients that depend on γ. From the system of differential equations for A and B, we find recursively at the cubic and quintic powers of A that

$$\begin{aligned} c_0 &= \frac{-1}{(\lambda_3^N - \lambda_1^N)^2 + 2\gamma}, \\ c_1 &= \frac{-3}{[(\lambda_3^N - \lambda_1^N)^2 + 2\gamma][(\lambda_3^N - \lambda_1^N)^2 + 4\gamma]}, \\ b_0 &= \frac{3}{[(\lambda_3^N - \lambda_1^N)^2 + 2\gamma][(\lambda_3^N - \lambda_1^N)^2 + 4\gamma]}. \end{aligned}$$

Substituting $B = \Psi_3(A, \bar{A})$ into the first equation of the system, we obtain consistently with (4.13) that the slow dynamics of A is given by

$$\dot{A} = A \left[\gamma - 3|A|^2 + \mathcal{O}(|A|^4) \right] - 3(b_0 + c_0^2)\bar{A}^7 \left[1 + \mathcal{O}(|A|^2) \right].$$

Since $r_{N=4} = -3(b_0 + c_0^2) < 0$, the nondegeneracy condition (4.15) is satisfied.

Remark 4.9 One can show with the method of mathematical induction that the nondegeneracy condition (4.15) is satisfied for every $N \geq 3$.

The following lemma is important for the persistence argument, when the discrete SHE is perturbed by a small correction term.

Lemma 4.10 *Let $u_\gamma^N, v_\gamma^N \in \mathbb{R}^{\mathbb{Z}_N}$ be defined by Theorem 4.2 for $\gamma \in (0, \gamma_0)$ under the nondegeneracy condition (4.15). Then, the matrix operator*

$$\mathcal{A}_\gamma := -(A_W^N - \lambda_1^N)^2 + \gamma - 3(u_\gamma)^2 : \mathbb{R}^{\mathbb{Z}_N} \to \mathbb{R}^{\mathbb{Z}_N},$$

where $(u_\gamma)^2$ is a diagonal matrix computed on the squared entries of u_γ^N, v_γ^N, is invertible.

Proof This follows from the available information about the eigenvalues of the linearized system (4.8) at the time-independent solutions $\{a_k\}_{k \in \mathbb{Z}_N}$ constructed from (4.13) with (4.12) and (4.14). Eigenvalues of the linearized system (4.17) are bounded away from zero and so are eigenvalues $-(\lambda_k^N - \lambda_1^N)^2$ for $k \neq \pm 1$. □

Remark 4.11 The inverse matrix $\mathcal{A}_\gamma^{-1}$ in Lemma 4.10 behaves poorly as $\gamma \to 0$ because the linearized system (4.17) has one eigenvalue $-2\gamma + \mathcal{O}(\gamma^2)$ and the other eigenvalue of $\mathcal{O}(\gamma^{N-1})$ under the nondegeneracy condition (4.15). As a result, $\|\mathcal{A}_\gamma^{-1}\| = \mathcal{O}(\gamma^{1-N}) \to \infty$ as $\gamma \to 0$.

5 The Discrete SHE on *W*-random Graphs

We now turn to the discrete SHE model (2.5) on the W-random graph $\tilde{\Gamma}_W^N$. Using (2.6), we rewrite it as follows

$$\dot{u} = -\left(\tilde{A}_W^N - \tilde{D}_W^N - \kappa\right)^2 u + \gamma u - u^3, \qquad j \in \mathbb{Z}_N, \tag{5.1}$$

where $u \in C^1(\mathbb{R}, \mathbb{R}^{\mathbb{Z}_N})$ and $\tilde{A}_W^N = (\tilde{a}_{ij})$ is the adjacency matrix of $\tilde{\Gamma}_W^N$. To make the setting for the model on a random graph consistent with the model on the deterministic Cayley graph, we have kept the periodic setting $\mathbb{Z}_N$ in (5.1). The matrix $\tilde{A}_W^N$ and the diagonal matrix $\tilde{D}_W^N$ act on components of $u \in \mathbb{R}^{\mathbb{Z}_N}$. The same notations $\tilde{A}_W^N$ and $\tilde{D}_W^N$ are used to denote the linear operators on $\mathbb{R}^{\mathbb{Z}_N}$.

We are interested in the Turing bifurcation of the trivial solution of (5.1). Appendix A shows that the matrix $\tilde{A}_W^N$ is close to the matrix A_W^N in the cut-norm with probability of $1 - \mathcal{O}(5^{-N})$. Consequently, eigenvalues of $\tilde{A}_W^N$ are close to the eigenvalues $\{\lambda_k^N\}_{k\in\mathbb{Z}_N}$ of A_W^N given by (4.4) (Szegedy (2011)). The following theorem presents the main result on the steady-state solutions in (5.1).

Theorem 5.1 *Assume that $\lambda_k^N \neq \lambda_1^N$ for $k \neq \pm 1$ and choose $\kappa := \lambda_1^N - d_W^N = \lambda_{-1}^N - d_N^W$. Fix $\gamma \in (0, \gamma_0)$ with γ_0 given in Theorem 4.2 and with $r_N \neq 0$ in (4.15). There exist $N_0 \geq 3$ such that with probability of $1 - \mathcal{O}(5^{-N})$, for every $N \geq N_0$ there exist at least 4 and at most $4N$ values of δ such that the discrete SHE (5.1) admits time-independent solutions $u \in \mathbb{R}^{\mathbb{Z}_N}$ satisfying*

$$\sup_{j\in\mathbb{Z}_N} \left| u_j - \frac{2}{\sqrt{3}}\sqrt{\gamma}\cos\left(\frac{\pi j}{N} - \delta\right)\right| \leq C_0\sqrt{\gamma^3}, \tag{5.2}$$

where the constant $C_0 > 0$ is independent of $N \geq N_0$ and $\gamma \in (0, \gamma_0)$.

Remark 5.2 The system (5.1) does not have any symmetries except of the symmetry with respect to the sign reflection $u \mapsto -u$. Theorem 4.2 gives existence and stability of two distinct state u_γ^N and v_γ^N for sufficiently small $\gamma > 0$, which are translated to every point of the lattice chain by the discrete translational symmetry of Lemma 4.1. Since the lattice chain in $\mathbb{Z}_N$ has $2N$ sites, we can count $4N$ distinct steady-state solutions in the discrete SHE model (4.1), of which $2N$ are stable and $2N$ are unstable. Compared to this conclusion, we do not have an exact count of the number of steady-state solutions on the random graph because of the broken symmetries. The number of steady solution is a random number between 4 and $4N$.

Remark 5.3 Recall that the matrix $\mathcal{A}_\gamma$ in Lemma 4.10 has a very small eigenvalue of the size $\mathcal{O}(\gamma^{N-1})$ for large $N \geq 3$. Due to this small eigenvalue, we cannot not prove that the steady-state solutions of (4.1) persist as the steady-state solutions of (5.1) because the perturbation is not sufficiently small, see Appendix A, and the Implicit Function Theorem cannot be used for the persistence argument. To overcome this problem, we develop again the approach based on the center manifold reduction, where the main difference is that the linear part of (5.1) is no longer diagonalizable by the discrete Fourier transform. The cubic nonlinear term still enjoys the same transformation under the discrete Fourier transform as in the proof of Theorem 4.2. The other distinction from the deterministic setting is that we can no longer use $\gamma > 0$ as a small continuation parameter. Instead, we consider the small parameter γ as fixed in $(0, \gamma_0)$ with γ_0 given in Theorem 4.2 and continue the solution with respect to an additional small parameter μ induced by randomness which is small for sufficiently large $N \geq N_0$.

Proof of Theorem 5.1 As in the proof of Theorem 4.2, we use discrete Fourier transform

$$u_j(t) = \sum_{k \in \mathbb{Z}_N} a_k(t) e^{\frac{i\pi kj}{N}}, \quad j \in \mathbb{Z}_N.$$

To apply the result in Appendix A, we write

$$u = Fa, \quad F = \left(\omega^{jk}\right)_{-N \leq j,k \leq N-1}, \quad \omega = e^{i\pi/N},$$

with $F^{-1} = (2N)^{-1} F^*$, where F^* stands for the conjugate transpose of F. By applying the inverse Fourier transform to both sides of (5.1), we have

$$\begin{aligned} \dot{a}_k = -(\hat{L}a)_k + \gamma a_k &- \sum_{-N \leq k_1,k_2,k-k_1-k_2 \leq N-1} a_{k_1} a_{k_2} a_{k-k_1-k_2} \\ &- \sum_{-N \leq k_1,k_2,k+2N-k_1-k_2 \leq N-1} a_{k_1} a_{k_2} a_{k+2N-k_1-k_2} \\ &- \sum_{-N \leq k_1,k_2,k-2N-k_1-k_2 \leq N-1} a_{k_1} a_{k_2} a_{k-2N-k_1-k_2}, \end{aligned} \tag{5.3}$$

where

$$\hat{L} = F^{-1} \left(\tilde{A}_W^N - \tilde{D}_W^N - \kappa\right)^2 F.$$

Recall that similarity transformation $A_W^N \mapsto F^{-1} A_W^N F$ diagonalizes the linear part of the deterministic model (4.1). Thus,

$$\hat{L} = \text{diag}\{(\lambda_{-N}^N - \lambda_1^N)^2\}, \ldots, (\lambda_{N-1}^N - \lambda_1^N)^2\} + \Delta, \tag{5.4}$$

where

$$\Delta = F^{-1}\left\{((2N)^{-1}\tilde{A}_W^N - \tilde{D}_W^N - \kappa)^2 - ((2N)^{-1}A_W^N - d_W^N - \kappa)^2\right\}F \tag{5.5}$$

and we have used that $\kappa = \lambda_1^N - d_W^N$. $\tilde{A}$ is a symmetric matrix, whose entries above the main diagonal are independent random variables. Further, $\mathbb{E}\tilde{A} = A$. From these facts, by Bernstein's inequality, it follows that with probability at least $1 - \mathcal{O}\left(25^{-N}\right)$, we have

$$\max_{-N\le j,k\le N-1} |\Delta_{jk}| \le C(\varsigma_N^3 N)^{-1/2} \tag{5.6}$$

(cf. Lemma A.1). Pick $\mu > 0$ small and fixed. It follows from (5.6) that with high probability for sufficiently large N, we have

$$\max_{-N\le j,k\le N-1} |\Delta_{jk}| \le \mu. \tag{5.7}$$

In order to incorporate the smallness of the bound (5.7) explicitly in the power expansions, we scale entries of Δ as $\Delta = \mu\tilde{\Delta}$, where $\max_{-N\le j,k\le N-1} |\tilde{\Delta}_{jk}| \le 1$ according to (5.7).

We apply the center manifold theorem (Haragus and Iooss (2011), Theorem 2.9). Since the spectrum of Δ is bounded uniformly in N (cf. (5.7)) and the cubic nonlinear terms are locally Lipschitz with constant independent on N, the domain of validity of the center manifold reduction can be chosen independently of N. As a result of the center manifold reduction, we express the slow manifold of the system (5.3) as the graph of functions $a_0 = \Psi_0(A, \bar{A})$, $a_1 = A$, $a_{-1} = \bar{A}$, and

$$a_k = \Psi_k(A, \bar{A}), \quad a_{-k} = \bar{\Psi}_k(A, \bar{A}), \quad k \in \{2, 3, \ldots, N\}.$$

In contrast to (4.12) $\hat{L}$ couples the odd-numbered and even-numbered Fourier amplitudes.

The functions $\Psi_k(A, \bar{A})$, $k \neq \pm 1$ can be obtained from the condition that γ and μ are small, whereas $(\lambda_k^N - \lambda_1^N)^2$ in $\hat{L}_{kk}$ are strictly positive and bounded away from zero for every $k \neq \pm 1$. The dynamics on the slow manifold can be expressed by the amplitude equation:

$$\dot{A} = F_1(A, \bar{A}), \quad \dot{\bar{A}} = \overline{F_1(A, \bar{A})}, \tag{5.8}$$

where F_1 is a C^∞ function in A and $\bar{A}$ with (γ,μ)-dependent coefficients. The Taylor series expansion includes only odd powers of A and $\bar{A}$ due to the only symmetry of the random model (5.1) with respect to the sign reflection $u \mapsto -u$.

The power expansion of $F_1(A, \bar{A})$ is different from those in the proof of Theorem 4.2 due to the presence of the perturbation terms $\Delta = \mu\tilde{\Delta}$ in (5.4). In addition, it is no longer true that $F_1(A, \bar{A})$ can be written in the form (4.13). Nevertheless, the nonzero

terms in the expansion of (4.13) remain dominant terms in the expansion of (5.8) if μ is sufficiently small. Thus, we have

$$\begin{aligned} F_1(A,\bar{A}) = (\gamma+\mu\alpha_1)A + \mu\alpha_2\bar{A} \\ + (-3+\mu\beta_1)|A|^2A + \mu\beta_2A^3 + \mu\beta_3|A|^2\bar{A} + \mu\beta_4\bar{A}^3 + \dots \\ + [r_N + \mathcal{O}(\mu)]\bar{A}^{2N-1} + \dots \end{aligned} \tag{5.9}$$

with some (γ,μ)-dependent coefficients which are bounded as $|\gamma|+|\mu|\to 0$. Since $\gamma\in(0,\gamma_0)$ is fixed and μ in (5.7) can be chosen sufficiently small, we have

$$\gamma+\mu\alpha_1 > 0, -3+\mu\beta_1 < 0, \text{ and } r_N+\mathcal{O}(\mu)\neq 0.$$

By using the polar form $A=\rho e^{i\theta}$, we write

$$\begin{cases} \dot{\rho} = [\gamma+\mu\alpha_1+\mu\alpha_2\cos(2\theta)]\rho \\ \qquad +[-3+\mu\beta_1+\mu\beta_2\cos(2\theta)+\mu\beta_3\cos(2\theta)+\mu\beta_4\cos(4\theta)]\rho^3+\mathcal{O}(\rho^5), \\ \dot{\theta} = -\mu\alpha_2\sin(2\theta)+\mu[\beta_2\sin(2\theta)-\beta_3\sin(2\theta)-\beta_4\sin(4\theta)]\rho^2+\dots \\ \qquad -[r_N+\mathcal{O}(\mu)]\rho^{2N-2}\sin(2N\theta)+\mathcal{O}(\rho^{2N}). \end{cases} \tag{5.10}$$

Since μ is selected to be much smaller than γ, there exists only one positive root of equation

$$\begin{aligned} \gamma+\mu\alpha_1+\mu\alpha_2\cos(2\theta)+[-3+\mu\beta_1+\mu\beta_2\cos(2\theta)+\mu\beta_3\cos(2\theta) \\ +\mu\beta_4\cos(4\theta)]\rho^2+\mathcal{O}(\rho^4)=0, \end{aligned}$$

which satisfies

$$\left|\rho-\frac{\sqrt{\gamma}}{\sqrt{3}}\right| \le C(\gamma+\mu\gamma^{-1})\sqrt{\gamma}, \tag{5.11}$$

with some constant $C>0$ which does not depend on $\gamma\in(0,\gamma_0)$ and $\theta\in[0,2\pi)$ as long as $\mu\ll\gamma$. The value of θ is defined from the second equation of system (5.10). Since there is no discrete translational symmetry of the system (5.1), compared to the system (4.1), we have to consider θ defined on $[0,2\pi)$. Roots of θ are defined from equation

$$\begin{aligned} -\mu\alpha_2\sin(2\theta)+\mu[\beta_2\sin(2\theta)-\beta_3\sin(2\theta)-\beta_4\sin(4\theta)]\rho^2+\dots \\ -[r_N+\mathcal{O}(\mu)]\rho^{2N-2}\sin(2N\theta)+\mathcal{O}(\rho^{2N})=0, \end{aligned} \tag{5.12}$$

where ρ satisfies the bound (5.11). Since the left-hand-side of (5.12) is a trigonometric polynomial in 2θ, there exist at least four roots of θ in $[0,2\pi)$ and at most $4N$ roots since $r_N+\mathcal{O}(\mu)\neq 0$. For each root of θ, the root of ρ in (5.11) is uniquely defined and the bound (5.2) with $\delta:=\frac{N}{\pi}\theta$ follows. □

Remark 5.4 The stability of steady states in Theorem 5.1 follows from the linearization of system (5.10) near each root and from the fact that all other eigenvalues of $-\hat{L}_\kappa$ are strictly negative of the order of $\mathcal{O}(1)$ for small γ and μ. Let (ρ_1, θ_1) be the perturbation terms to the root (ρ, θ) which satisfy linearized equations obtained from linearization of the system (5.10). The linearized evolution in ρ_1 is asymptotically stable. In a generic situation, when all roots of the trigonometric polynomial in (5.12) are simple, the linearized evolution in θ_1 is asymptotically stable for half of solutions and is unstable for the other half of solutions.

Remark 5.5 Coefficients α_1 and α_2 in (5.9) can be easily computed from the linear part of system (5.3). Since $\Psi_k(A, \bar{A}) = \mathcal{O}(\mu)|A|$ for $k \neq \pm 1$, we have at the leading order:

$$\mu\alpha_1 = \Delta_{1,1} + \mathcal{O}(\mu^2), \quad \mu\alpha_2 = \Delta_{1,-1} + \mathcal{O}(\mu^2),$$

where $\Delta_{1,\pm 1} = \mu\tilde{\Delta}_{1,\pm 1}$ with $\tilde{\Delta}_{1,\pm 1}$ being of the order of $\mathcal{O}(1)$ as $\mu \to 0$, see (5.7).

Remark 5.6 If $\tilde{\Delta}_{1,-1} \neq 0$ in $\alpha_2 = \tilde{\Delta}_{1,-1} + \mathcal{O}(\mu)$, we have exactly four time-independent solutions, from which two are asymptotically stable and two are unstable. The two stable (or unstable) solutions are related to each other by the sign reflection symmetry $u \mapsto -u$ of the discrete SHE (5.1). This follows from the fact that the center manifold reduction relies on a trigonometric polynomial in 2θ for which θ_0 and $\pi + \theta_0$ are equivalent points. If $\Delta = 0$ in (5.4), then we have $4N$ time-independent solutions, identically to Theorem 4.2.

Remark 5.7 In comparison with Theorem 4.1 in Bramburger and Holzer (2023), we do not include the quadratic terms in the discrete SHE models to avoid technical computations of the near-identity transformations. We also specify the particular case $k_0 = 1$ in Theorems 4.2 and 5.1 to simplify computations of the normal forms. On the other hand, we give a precise statement of how the translational parameter δ of Theorem 3.8 is determined in the case of the discrete graphs (both in the deterministic and random cases) and how many time-independent solutions exist for the discrete graph models. In addition, the proof of Theorem 4.1 in Bramburger and Holzer (2023) is incomplete. The analysis of the Fourier mode w_2 corresponding to the small eigenvalue $l_2 = -\delta^2 N^2 \rho_2$ is not included in the proof. In our setting, the dynamics of w_2 is captured by the equation for θ in (5.10). This equation is important, because it determines the number of branches bifurcating from the spatially homogeneous equilibrium.

6 The Discrete SHE on Small-World Graphs

In this section, we illustrate the bifurcation analysis of the discrete SHE models on the deterministic and random graphs with numerical results. To this end, we use the family of small-world graphs from Example 2.1. This is a representative example, for which Assumption 3.6 can be verified analytically.

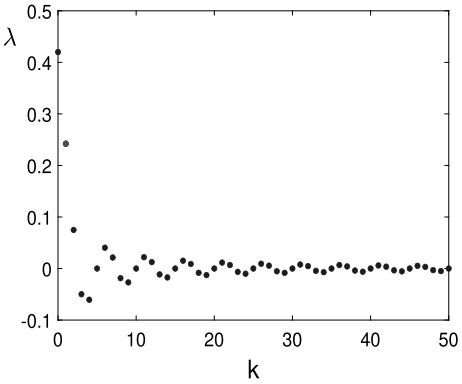

Fig. 2 Eigenvalues of K_S given by (6.2) for $N = 50$, $p = 0.1$ and $r = 0.2$

Recall the definition of the small-world graphon $W(x, y) = S(x - y)$ with $S \in L^1(\mathbb{T})$ given by

$$S(x) = \begin{cases} 1 - p, & |x| \le r, \\ p, & r < |x| \le \frac{1}{2}, \end{cases} \tag{6.1}$$

where $p \in [0, 1]$ and $r \in \left(0, \frac{1}{2}\right)$. The eigenvalues of the Hilbert-Schmidt operator K_S in (3.2) are known explicitly (cf. Medvedev (2014c); Chiba and Medvedev (2019)):

$$\lambda_k = \begin{cases} 2r(1 - 2p) + p, & k = 0, \\ (\pi k)^{-1}(1 - 2p) \sin(2\pi k r), & k \in \mathbb{Z}\backslash\{0\}. \end{cases} \tag{6.2}$$

Eigenvalues are shown in Fig. 2 for $N = 50$, $p = 0.1$ and $r = 0.2$. It is clear from the figure that $\lambda_k < \lambda_1$ for $k \ge 2$ so that Assumption 3.6 is satisfied with $\kappa = \lambda_1 - d_S$ and $d_S = \lambda_0$.

By Theorem 3.8, for small $\gamma > 0$, the continuous SHE model (3.1) has a continuous family of asymptotically orbitally stable solutions $\{u_\gamma(\cdot + \delta)\}_{\delta \in \mathbb{T}}$, where u_γ is approximated by

$$u_\gamma(x) = 2\sqrt{\frac{\gamma}{3}} \cos(2\pi x) + \mathcal{O}(\gamma^{3/2}). \tag{6.3}$$

We shall now consider how the stable solutions with the expansion (6.3) persist in the discrete SHE models on the deterministic and random graphs. For the discrete SHE model (4.1) with (4.2) and (6.1), we compute the eigenvalues of A_W^N in the form

$$\lambda_k^N = \frac{1 - p}{2N} \sum_{|j| \le \lceil rN \rceil} e^{\frac{-i\pi kj}{N}} + \frac{p}{2N} \sum_{|j| > \lceil rN \rceil} e^{\frac{-i\pi kj}{N}}.$$

We set $\kappa = \lambda_1^N - d_W^N$ with $d_W^N = \lambda_0^N$. For small $\gamma > 0$, Theorem 4.2 yields existence of the two discrete families of solutions $\{\sigma_m u_\gamma^N\}_{m \in \mathbb{Z}_N}$ and $\{\sigma_m v_\gamma^N\}_{m \in \mathbb{Z}_N}$, where σ_m is

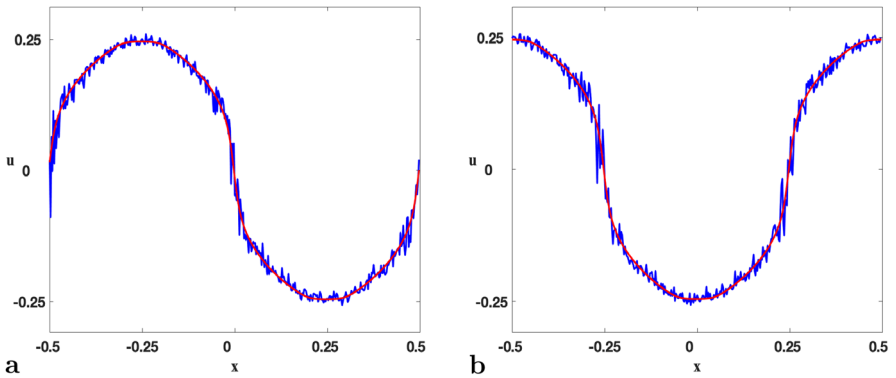

Fig. 3 Numerical solutions of the SHE on deterministic SHE with kernel (6.1) with parameters $N = 400$, $p = 0.1$, $r = 0.2$, and $\gamma = 0.05$ plotted in red and its random counterpart plotted in blue. Both models were initialized with the discretization of the leading-order term in (6.3) and integrated for 100 units of time. The shift δ was set to $-\pi/2$ in plot **a** and to 0 in plot **b**

the shift operator defined by $(\sigma_m u)_j = u_{j+m}$, $j \in \mathbb{Z}_N$ and the profiles of u_γ^N and v_γ^N are approximated, respectively, by

$$u_j = \frac{2}{\sqrt{3}}\sqrt{\gamma}\cos\left(\frac{\pi j}{N}\right) + \mathcal{O}\left(\gamma^{3/2}\right), \tag{6.4}$$

$$v_j = \frac{2}{\sqrt{3}}\sqrt{\gamma}\cos\left(\frac{\pi j}{N} - \frac{\pi}{2N}\right) + \mathcal{O}\left(\gamma^{3/2}\right), \tag{6.5}$$

for $j \in \mathbb{Z}_N$. One of the two solutions is asymptotically stable and the other solution is unstable.

The random SHE model (5.1), we use the same κ and define the symmetric matrix $\tilde{A}_W^N$ with zeros on the main diagonal and with the entries above the main diagonal $\tilde{a}_{ij}^N$ being independent random variables such that

$$\mathbb{P}(\tilde{a}_{ij}^N = 1) = a_{ij}^N, \qquad \text{and} \qquad \mathbb{P}(\tilde{a}_{ij}^N = 0) = 1 - a_{ij}^N,$$

where a_{ij}^N is a coefficient of the adjacency matrix of the weighted Cayley graph. Theorem 5.1 implies the existence of asymptotically stable solutions with the approximation

$$u_{\gamma,\delta} = \frac{2}{\sqrt{3}}\sqrt{\gamma}\cos\left(\frac{\pi j}{N} - \delta\right) + \mathcal{O}\left(\gamma^{3/2}\right) \tag{6.6}$$

for small $\gamma > 0$ and appropriate fixed δ.

Figure 3 presents results of numerical simulations of the discrete models derived from the nonlocal SHE with kernel (6.1) with parameters $N = 400$, $p = 0.1, r = 0.2$, and $\gamma = 0.05$. Both the deterministic and random models were initialized with the leading-order term on the right-hand side of (6.3). The shift δ was set to $-\pi/2$ in plot **a** and to 0 in plot **b**. The two models were integrated for 100 units of time. The solutions

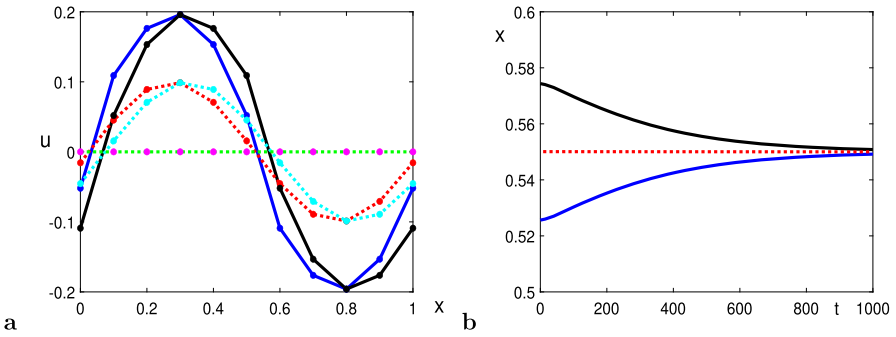

Fig. 4 Numerical approximations of the discrete SHE model (4.1) for $N = 5$, $p = 0.9$, $r = 0.2$, and $\gamma = 0.03$. **a** Two initial conditions (red and cyan lines) and the outcomes of numerical simulations at $t = 100$ (blue and black lines). **b** Numerically obtained zeros of the two solutions versus time relative to the midpoint between two grid points (red dotted line)

of the deterministic models are plotted in red and the solutions of the random model are plotted in blue.

On finite time intervals, the solutions of the discrete SHE on deterministic and random graphs are expected to remain close, provided the initial data are sufficiently close and N is large (cf. Medvedev (2019)). This is clearly seen in the simulations shown in Fig. 3. The snapshots of the trajectories of the deterministic and the random models, shown in red and blue, respectively, lie very close to each other. For the deterministic model, we know that the trajectory relaxes to one of the $2N$ stable states lying in the vicinity of the initial condition. As to the snapshots of the SHE on random graph, we see that they relax to the form predicted by Theorem 5.1.

Remark 6.1 Since $(4N)$ steady states of the discrete model (4.1), of which $(2N)$ are asymptotically stable, are packed on the bounded interval, the numerical computations in Fig. 3 would not distinguish where the $2N$ stable solutions are pinned with respect to the lattice sites if N is large. Note that the evolution in the translational direction is extremely slow due to the $O(\gamma^{N-1})$ eigenvalue, and cannot be resolved by numerics for large N. In order to illustrate the effects of the slow drift in numerical simulations, we performed computations of the deterministic and random SHE models for $N = 5$, for which these effects can be demonstrated numerically.

Figure 4 shows outcomes of the numerical simulations for the discrete SHE model (4.1) with two different initial conditions given by the red and cyan dotted lines. The two initial data are given by (6.3) with a half of the amplitude and shifted to the right and to the left relative to the grid points (shown by magenta dots). The two solutions quickly converge to the near-equilibrium solutions with the correct amplitude of 0.2 (blue and black solid lines) which then slowly shift further from the grid points toward the mid-point between the two grid points. The snapshot on the left panel was made at time $t = 100$, but the slow drift of the zeros of the two solutions on the much longer time interval is shown on the right panel. Zeros are computed from the linear interpolation between the grid points and the color scheme is the same as that for the final states on

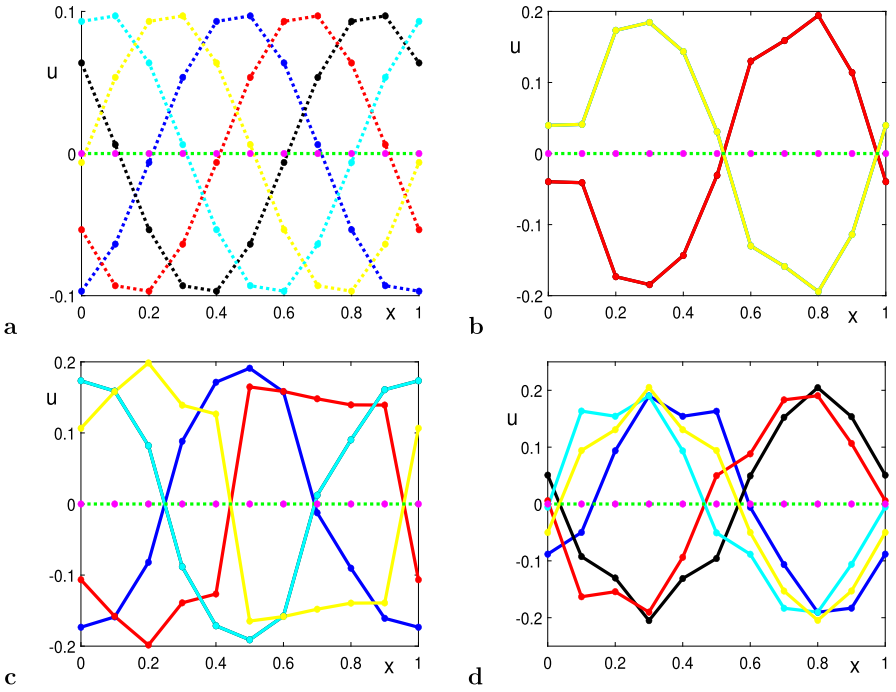

Fig. 5 Numerical approximations of random realizations of the discrete SHE model (5.1) for $N = 5$, $p = 0.9$, $r = 0.2$, and $\gamma = 0.03$. **a** Five initial conditions shifted relative to each other. **b–d** Outcomes of numerical simulations with two, four, and six stable solutions

the left panel. This numerical experiment shows that the asymptotically stable solution is given by a discrete translation of the solution v_γ^N given by the expansion (6.5).

Figure 5 shows outcomes of the numerical simulations for the random realizations of the discrete SHE model (5.1) with five different initial conditions shown on the top left panel. The drift generally occurs faster in the random model because the relevant small eigenvalue is of the size $\mathcal{O}(\mu)$ if $\alpha_2 \neq 0$ (see (5.10)), where μ is defined by (5.7). Only two time-independent solutions are stable if $\alpha_2 \neq 0$ and this generic case is shown on the top right panel. The two stable solutions are given by (6.6) with some specific δ and they are related by the sign reflection of each other. The color scheme of the final states corresponds to that of the initial conditions and the missing colors correspond to the final states identical to those shown in red and yellow.

If α_2 is zero or close to zero, then four, six, eight, or ten time-independent solutions could be stable according to Theorem 5.1 and since half states are related by the sign reflection of the other half states, five numerical conditions could be used to detect all cases. However, the cases with more stable states are rare. Our numerical simulations showed random configuration of the discrete SHE model with four and six stable states (bottom left and right panels, respectively), but we did not find random configurations with eight and ten stable states. The four configurations on the bottom left panel shows that two states are given by the sign reflection of the other two states (red versus yellow and blue versus cyan). The same is true for the bottom right panel (red versus cyan and

black versus yellow), but there is one more stable state (blue line) which is not matched by the sign reflected state (since our simulations only involve five initial conditions).

7 Discussion

Dynamical principles underlying formation of patterns in complex systems are important for understanding a range of phenomena arising across multiple disciplines from morphogenesis to autocatalytic reactions, to firing patterns in neuronal networks (Murray 1989). Traditionally, pattern formation has been predominantly studied in the continuous setting through the framework of reaction-diffusion partial differential equations. Recently, the interest has shifted toward understanding patterns in discrete systems, driven by the ubiquity of networks in contemporary science. Interestingly, already in his seminal paper on morphogenesis, Turing considered a reaction-diffusion model on a lattice, i.e., a discrete system (Turing 1952). There is an extensive literature on lattice dynamical systems, which covers pattern formation and propagation phenomena (Han and Kloeden 2023). In the past decade, there have been many studies exploring pattern formation in complex networks including random networks. The key analytical challenge in dealing with this class of models, which was not present in studies of partial differential equations or lattice dynamical systems, is handling network topology, which can be random. Until recently most studies of the dynamics of complex and random networks had to resort to heuristic and numerical arguments (see Nakao and Mikhailov (2010); Wolfrum (2012); Hütt et al. (2022); Asllani et al. (2014); Kouvaris et al. (2015) for a representative albeit limited sample of studies of Turing patterns in networks).

The situation has changed with the development of the theory of graphons (Lovász 2012). The use of graphons allows a rigorous derivation of the continuum limit for interacting dynamical systems on a large class of graphs including random graphs (Medvedev 2014a, b, 2019), which can be used effectively for studying dynamics on large networks. For example, the use of graphons led to the breakthrough in the analysis of synchronization and pattern formation in systems of coupled phase oscillators on networks (Chiba et al. 2023; Medvedev and Mizuhara 2022), interacting diffusions on graphs (Oliveira et al. 2020; Luçon 2020), mean-field games (Caines and Huang 2021), and graph signal processing (Ruiz et al. 2020; Ghandehari et al. 2022).

Graphons provide multiple analytical benefits. Oftentimes, graph limits possess additional symmetries that are not present in the individual realizations of random graphs. For example, the graph limit of the small-world family of graphs used in the present work is isotropic, in contrast to the graphons corresponding to the realizations of small-world graphs. This symmetry enables the effective use of the Fourier transform for analyzing the limiting model (cf. Sect. 3).

Likewise, the deterministic (averaged) discrete model (4.1) is shift invariant and can be studied using discrete Fourier transform (cf. Sect. 4). This in turn can be used to understand the dynamics of the random model (5.1). In general, the proximity in cut norm of a network to a symmetric network can facilitate the analysis of the original nonsymmetric model.

In the context of the bifurcation problems considered in this paper, the relationship between the spectra and eigenspaces of the deterministic and random discrete models, as well as their continuum counterpart, is crucial. The theory of graph limits offers very efficient tools for tracking this relation. The convergence of kernel operators in cut-norm automatically implies the proximity of the corresponding eigenvalues and eigenspaces (Szegedy 2011). This has significant implications for the analysis of dynamical systems. For instance, once the proximity in cut norm of the linear operators corresponding to the interaction terms of the random model and its deterministic counterpart was verified (cf. Appendix A), the proximity of the eigenvalues and the corresponding eigenspaces followed automatically. In contrast, the analysis in Bramburger and Holzer (2023) based on operator norm topology and Davis–Kahan estimates requires substantial efforts. Importantly, the analysis in the present paper extends to sparse networks.

Our techniques apply naturally to other pattern–forming systems on random graphs, including Gierer–Meinhardt model (Hütt et al. 2022), Mimura–Murray model of interacting prey-predator populations (Nakao and Mikhailov 2010) and many other activator–inhibitor systems. An interesting area of potential applications are neural fields (Coombes et al. 2014). Fourier methods played an important role in the analysis of pattern in nonlocal neural field models, which are very similar to the continuum limit analyzed in Sect. 3 (Laing and Troy 2003). We expect that the methods developed this paper may lead to interesting results for discrete neural fields with random connectivity. Finally, the concentration estimate for the random linearized operator in Fourier space (cf. Appendix A) may be useful in graph signal processing.

8 Appendix A: A Concentration Inequality

Let $A = (a_{ij}) \in \mathbb{R}^{n\times n}$ be a symmetric matrix such that $0 \le a_{ij} \le 1$ and $a_{ii} = 0,\ i \in [n]$, and let $\tilde{A} = (\tilde{a}_{ij}) \in \mathbb{R}^{n\times n}$ such that $\tilde{a}_{ij},\ 1 \le i < j \le n$ are independent random variables defined as follows

$$\mathbb{P}(\tilde{a}_{ij} = \varsigma_n^{-1}) = \varsigma_n a_{ij}, \qquad \mathbb{P}(\tilde{a}_{ij} = 0) = 1 - \varsigma_n a_{ij},$$

and $\tilde{a}_{ij} = a_{ji},\ \tilde{a}_{ii} = 0$. Here, ς_n is a positive sequence satisfying

$$1 \ge \varsigma_n \ge Mn^{-1/3}, \tag{A.1}$$

for some $M > 0$ dependent of N. Further, define

$$D = \mathrm{diag}(d_1, d_2, \ldots, d_n), \quad d_i = n^{-1}\sum_{j=1}^{n} a_{ij},$$

$$\tilde{D} = \mathrm{diag}(\tilde{d}_1, \tilde{d}_2, \ldots, \tilde{d}_n), \quad \tilde{d}_i = n^{-1}\sum_{j=1}^{n} \tilde{a}_{ij},$$

and $\mathbf{A} = n^{-1}A$, $\tilde{\mathbf{A}} = n^{-1}A$. Consider

$$\Delta = F^{-1}\left\{(\mathbf{A} - D - \kappa)^2 - (\tilde{\mathbf{A}} - \tilde{D} - \kappa)^2\right\}F, \tag{A.2}$$

where

$$F = \left(\omega^{-(j-1)(k-1)}\right)_{1\le j,k\le n}, \qquad \omega \doteq e^{\frac{i2\pi}{n}}, \qquad F^{-1} = n^{-1}F^*.$$

The main result of this appendix is the following lemma with the straightforward corollary.

Lemma A.1 *With probability at least* $1 - O\left(5^{-n}\right)$,

$$\max_{1\le j,k\le n} |\Delta_{jk}| \le C(\varsigma_n^3 n)^{-1/2},$$

where C does not depend on n.

Corollary A.2 *For a given* $\epsilon > 0$ *with high probability, for all sufficiently large n,*

$$\max_{1\le j,k\le n} |\Delta_{jk}| \le \epsilon,$$

provided M in (A.1) is large enough.

We precede the proof of Lemma A.1 with a few comments. By construction of $\tilde{A}$, $\tilde{a}_{ij}$, $1 \le i < j \le n$ are independent random variables, $\mathbb{E}\tilde{A} = A$, and

$$p \doteq \frac{2}{n(n-1)}\sum_{i<j}\mathrm{Var}\,\varsigma_n\tilde{a}_{ij} = \frac{2}{n(n-1)}\sum_{i<j}\varsigma_n a_{ij}\left(1 - \varsigma_n a_{ij}\right). \tag{A.3}$$

Note that

$$p \simeq \begin{cases} \frac{1}{2}\int_Q W(1-W)\mathrm{d}x + o(1), & \varsigma_n \equiv 1 \quad \text{(dense case)},\\ \varsigma_n\frac{1}{2}\int_Q W\mathrm{d}x + o(1), & \varsigma_n \searrow 0 \quad \text{(sparse case)}. \end{cases}$$

In either case,

$$C_1\varsigma_n \le p \le C_2\varsigma_n \tag{A.4}$$

for appropriate positive C_1, C_2 independent of n.

The proof of Lemma A.1 relies on the estimates of $\left\|\tilde{\mathbf{A}} - \mathbf{A}\right\|_{\infty\to 1}$ and $\left\|\tilde{D} - D\right\|_{\infty\to 1}$ based on the Bernstein inequality (cf. (Guédon and Vershynin (2016), Theorem 4.3)). Here, the $\infty \to 1$ norm of $A \in \mathbb{R}^{n\times n}$ is defined as follows

$$\|A\|_{\infty\to 1} \doteq \max_{x,y\in\{-1,1\}^n}\left|\sum_{i,j=1}^n a_{ij}x_i y_j\right|. \tag{A.5}$$

In particular, for $X \in \{\mathbf{A}, D\}$, we have

$$\left\| \tilde{X} - X \right\|_{\infty \to 1} \leq 3\varsigma_n^{-1} p^{1/2} n^{3/2} \simeq \varsigma_n^{-1/2} n^{3/2}. \tag{A.6}$$

holding with probability at least $1 - e^3 5^{-n}$ provided

$$p > \frac{9}{n}.$$

For $X = \mathbf{A}$ (A.6) follows from Lemma 4.1 in Guédon and Vershynin (2016) and (A.4) For $X = D$ (A.6) is proved by following the same steps as in the proof of Lemma 4.1 in Guédon and Vershynin (2016).

Proof of Lemma A.1 We rewrite (A.2) as follows

$$\begin{aligned} \Delta = & F^{-1}\left(\tilde{\mathbf{A}}^2 - \mathbf{A}^2\right) F - 2\kappa F^{-1}\left(\tilde{\mathbf{A}} - \mathbf{A}\right) F \\ & - F^{-1}\left(\tilde{\mathbf{A}} - \mathbf{A}\right) \tilde{D} F - F^{-1}\mathbf{A}\left(\tilde{D} - D\right) F \\ & - F^{-1} D\left(\tilde{\mathbf{A}} - \mathbf{A}\right) F - F^{-1}\left(\tilde{D} - D\right) \mathbf{A} F. \end{aligned} \tag{A.7}$$

Denote the six terms in the order as they appear on the right hand side of (A.7) by $F^{-1} S_i F$, $i \in [6]$. We claim for each $i \in [6]$,

$$\left\| F^{-1} S_i F \right\|_{\infty} \leq C(\varsigma_n^3 n)^{-1/2} \tag{A.8}$$

holding with probability $1 - O(5^{-n})$. Once we verify (A.8), the proof will be complete. We verify (A.8) only for $i = 1, 2$, as the remaining terms are estimated in the same manner.

We start with the second term on the right hand side of (A.7)

$$\begin{aligned} \left| \left(F^{-1}\left(\tilde{\mathbf{A}} - \mathbf{A}\right) F\right)_{ij} \right| &= n^{-2} \left| \sum_{l,k} F_{il} \left(\tilde{A} - A\right)_{lk} F_{kj} \right| \leq 4n^{-2} \max_{x,y \in \{-1,1\}^n} \left| \sum_{l,k} x_l \left(\tilde{A} - A\right)_{lk} y_k \right| \\ &= n^{-2} \|A - \tilde{A}\|_{\infty \to 1} \leq C(\varsigma_n n)^{-1/2}, \end{aligned}$$

where we used $F^{-1} = nF^*$, $|F_{kl}| = 1$, and (A.6).

We now turn to the first term

$$F^{-1}\left(\tilde{\mathbf{A}}^2 - \mathbf{A}^2\right) F = n^{-3} F^* \left(\tilde{A}^2 - A^2\right) F$$

In this case, we need to estimate,

$$n^{-3} F^* \left(\tilde{A}^2 - A^2\right) F = n^{-3} F^* \tilde{A} \left(\tilde{A} - A\right) F + n^{-3} F^* \left(\tilde{A} - A\right) A F. \tag{A.9}$$

We estimate the first term on the right hand side of (A.9). The second term is dealt with similarly. Let

$$E = n^{-3} F^* \tilde{A} \left(\tilde{A} - A \right) F = \varsigma_n^{-1} n^{-3} F^* (\varsigma_n \tilde{A}) \left(\tilde{A} - A \right) F \tag{A.10}$$

Denote

$$\begin{aligned} x &= \mathrm{col}_i \left(n^{-1} \varsigma_n \tilde{A} F \right) = n^{-1} (\varsigma_n \tilde{A}) \, \mathrm{col}_i (F^*), \\ y &= \mathrm{col}_j (F). \end{aligned}$$

Note $\|x\|_\infty \le 1$. Thus,

$$\begin{aligned} \left| E_{ij} \right| &= \varsigma_n^{-1} n^{-2} \left| \sum_{i,j} x_i \left(\tilde{A} - A \right)_{ij} y_j \right| \\ &\le 4 \varsigma_n^{-1} n^{-2} \left\| \tilde{A} - A \right\|_{\infty \to 1} \le C \frac{1}{(\varsigma_n^3 n)^{1/2}}. \end{aligned}$$

This completes the analysis of S_1, the first term on the right hand side of (A.7). The remaining terms are analyzed similarly and result in either $O\left((\varsigma_n n)^{-1/2}\right)$ bound as for S_2 above or in $O\left((\varsigma_n^3 n)^{1/2}\right)$ bound for S_1. Thus, $\|\Delta\|_\infty = O\left((\varsigma_n^3 n)^{1/2}\right)$ as claimed. □

Remark A.3 Note that $O\left((\varsigma_n^3 n)^{1/2}\right)$ come from quadratic terms like S_2. If the second-order nonlocal spatial operator in (3.1) is replaced with the first-order operator (3.2), as one encounters in the neural field type models, then the bound on $\|\Delta\|_\infty$ can be improved to $O\left((\varsigma_n n)^{1/2}\right)$. This means that the results of this paper would hold for $\varsigma_n = O(n^{-1})$, i.e., for graphs of *bounded degree*.

Acknowledgements This work was partially supported by NSF grant DMS 2009233 (to G.S.M.) and NSERC Discovery grant (to D.E.P.).

Author Contributions G.S.M. and D.E.P. contributed to writing the manuscript equally. All authors reviewed the manuscript.

Data Availability No datasets were generated or analysed during the current study.

Declarations

Competing interests The authors declare no competing interests.

References

Asllani, M., Busiello, D.M., Carletti, T., Fanelli, D., Planchon, G.: Turing patterns in multiplex networks. Phys. Rev. E **90**, 042814 (2014)

Bramburger, J., Holzer, M.: Pattern formation in random networks using graphons. SIAM J. Math. Anal. **55**(3), 2150–2185 (2023)

Caines, P.E., Huang, M.: Graphon mean field games and their equations. SIAM J. Control. Optim. **59**(6), 4373–4399 (2021)

Cazenave, T., Haraux, A.: An Introduction to Semilinear Evolution Equations. Oxford University Press, Oxford (1998)

Chiba, H., Medvedev, G.S.: The mean field analysis of the Kuramoto model on graphs I. The mean field equation and transition point formulas. Discrete Contin. Dyn. Syst. **39**(1), 131–155 (2019)

Chiba, H., Medvedev, G.S., Mizuhara, M.S.: Bifurcations and patterns in the Kuramoto model with inertia. J. Nonlinear Sci. **33**(5), 21 (2023)

Chossat, P., Lauterbach, R.: Methods in Equivariant Bifurcations and Dynamical Systems. World Scientific Publishing Co. Inc, River Edge, NJ (2000)

Collet, P., Eckmann, J.P.: Instabilities and Fronts in Extended Systems. Princeton University Press, Princeton, NJ (1990)

Coombes, S., Graben, P., Potthast, R.: Tutorial on Neural Field Theory, pp. 1–43. Neural fields, Springer, Heidelberg (2014)

Dorfler, F., Bullo, F.: Synchronization and transient stability in power networks and non-uniform Kuramoto oscillators. SICON **50**(3), 1616–1642 (2012)

Ghandehari, M., Janssen, J., Kalyaniwalla, N.: A noncommutative approach to the graphon Fourier transform. Appl. Comput. Harmon. Anal. **61**, 101–131 (2022)

Guédon, O., Vershynin, R.: Community detection in sparse networks via Grothendieck's inequality. Probab. Theory Related Fields **165**(3–4), 1025–1049 (2016)

Han, X., Kloeden, P.: Dissipative Lattice Dynamical Systems. Interdisciplinary Mathematical Sciences, vol. 22, World Scientific Publishing Co. Pte. Ltd., Hackensack, NJ (2023)

Haragus, M., Iooss, G.: Local Bifurcations, Center Manifolds, and Normal Forms in Infinitedimensional Dynamical Systems. Universitext, Springer-Verlag London, Ltd., EDP Sciences, London, Les Ulis (2011)

Hupkes, H.J., Pelinovsky, D.E., Sandstede, B.: Propagation failure in the discrete nagumo equation. Proc. AMS **139**, 3537–3551 (2011)

Hütt, M.-T., Armbruster, D., Lesne, A.: Predictable topological sensitivity of turing patterns on graphs. Phys. Rev. E **105**, 014304 (2022)

Kouvaris, N., Hata, S., Guilera, A.: Pattern formation in multiplex networks. Sci. Rep. **5**, 10840 (2015)

Laing, C.R., Troy, W.C.: Pde methods for nonlocal models. SIAM J. Appl. Dyn. Syst. **2**(3), 487–516 (2003)

Lovász, L.: Large Networks and Graph Limits. AMS, Providence, RI (2012)

Lovász, L., Szegedy, B.: Limits of dense graph sequences. J. Combin. Theory Ser. B **96**(6), 933–957 (2006)

Luçon, E.: Quenched asymptotics for interacting diffusions on inhomogeneous random graphs. Stochastic Process. Appl. **130**(11), 6783–6842 (2020)

Medvedev, G.S.: The nonlinear heat equation on dense graphs and graph limits. SIAM J. Math. Anal. **46**(4), 2743–2766 (2014a)

Medvedev, G.S.: The nonlinear heat equation on W-random graphs. Arch. Ration. Mech. Anal. **212**(3), 781–803 (2014b)

Medvedev, G.S.: Small-world networks of Kuramoto oscillators, Phys. D **266**, 13–22. MR3129708 (2014c)

Medvedev, G.S.: The continuum limit of the Kuramoto model on sparse random graphs. Commun. Math. Sci. **17**(4), 883–898 (2019)

Medvedev, G.S., Mizuhara, M.S.: Chimeras unfolded. J. Stat. Phys. **186**(3), Paper No. 46, 19 (2022)

Medvedev, G.S., Tang, X., The Kuramoto model on power law graphs: Synchronization and contrast states. J Nonlinear Sci **30**, 2405–2427 (2020)

Murray, J.D.: Mathematical Biology, Biomathematics, vol. 19. Springer-Verlag, Berlin (1989)

Nakao, H., Mikhailov, A.: Turing patterns in network-organized activator-inhibitor systems. Nat. Phys. **6**, 544–550 (2010)

Oliveira, R. I., Reis, G. H., Stolerman, L.M.: Interacting diffusions on sparse graphs: hydrodynamics from local weak limits. Electron. J. Probab. **25**, 1–35 (2020)

Pikovsky, A., Rosenblum, M., Kurths, J..: Synchronization: A universal concept in nonlinear sciences. Cambridge Nonlinear Science Series, vol. 12, Cambridge University Press, Cambridge (2001)
Porter, M.A., Gleeson, J.P.: Dynamical Systems on Networks, Frontiers in Applied Dynamical Systems: Reviews and Tutorials, vol. 4. Springer, Cham. A tutorial (2016)
Ruiz, L., Chamon, L.F.O., Ribeiro, A.: Graphon signal processing. IEEE Trans. Signal Process. **69**, 4961–4976 (2020)
Strogatz, S.: How Order Emerges from Chaos in the Universe, Nature, and Daily Life. Hyperion Books, New York (2003)
Szegedy, B.: Limits of kernel operators and the spectral regularity lemma. Eur. J. Combin. **32**(7), 1156–1167. (2011)
Turing, A.M.: The chemical basis of morphogenesis. Philos. Trans. R. Soc. B **237**(641), 37–72 (1952)
Watts, D.J., Strogatz, S.H.: Collective dynamics of small-world networks. Nature **393**, 440–442 (1998)
Wiley, D.A., Strogatz, S.H., Girvan, M.: The size of the sync basin. Chaos **16**(1), 015103, 8. (2006)
Wolfrum, M.: The Turing bifurcation in network systems: collective patterns and single differentiated nodes. Physica D **241**(16), 1351–1357 (2012)